Russian Chemical Reviews **78** (8) 717 – 736 (2009) © 2009 Russian Academy of Sciences and Turpion Ltd

DOI 10.1070/RC2009v078n08ABEH004061

Application of modern NMR techniques for conformational analysis of oligo- and polysaccharides

A A Grachev, A G Gerbst, A S Shashkov, N E Nifantiev

Contents

I. Introduction 717
II. Structural and spectral (NMR) characteristics used in the conformational analysis of oligo- and polysaccharides 717
III. Modern methods for the determination of spin – spin coupling constants and specific aspects of their use in conformational analysis of oligo- and polysaccharides 718
IV. Modern methods for registration of the nuclear Overhauser effect and specific aspects of its use in conformational analysis of oligo- and polysaccharides 729
V. Conclusion 735

Abstract. Application of modern NMR techniques for the determination of spin – spin coupling constants and nuclear Overhauser effect is addressed, as well as the use of these data in experimental conformational analysis of oligo- and polysaccharides. The bibliography includes 95 references.

I. Introduction

The development of methods for conformational analysis of oligo- and polysaccharides started in the 1970 – 1980s and was associated with the fundamental works in the field of glycobiology, which demonstrated the exceptionally important role of carbohydrate derivatives in many processes of cell recognition. It is at that time that the structures of many classes of carbohydrate compounds were established, in particular, of blood group determinants,[1,2] microbial polysaccharides,[3,4] glycolipids, glycoproteins and others.[5] The classical studies of biosynthesis of complex natural glycoconjugates[6] and the mechanism of their recognition by different types of carbohydrate-binding proteins were carried out.[7–9] This formed the basis for further successful investigations of the role of natural glycoconjugates in thrombogenesis, tumorigenesis and metastases, inflammations, microbial infections and other serious diseases.[10–17] Understanding of the mechanisms of the origin and the course of the mentioned processes at the molecular level can serve as a tool for drug research and structure optimization.[18]

A A Grachev, A G Gerbst, A S Shashkov, N E Nifantiev N D Zelinsky Institute of Organic Chemistry, Russian Academy of Sciences, Leninsky prosp. 47, 119991 Moscow, Russian Federation. Fax (7-499) 135 87 84, tel. (7-499) 135 64 33, e-mail: grachevaa@mail.ru (A A Grachev), alger@ioc.ac.ru (A G Gerbst), tel. (7-499) 135 90 94, e-mail: shash@ioc.ac.ru (A S Shashkov), tel. (7-499) 135 87 84, e-mail: nen@ioc.ac.ru (N E Nifantiev)

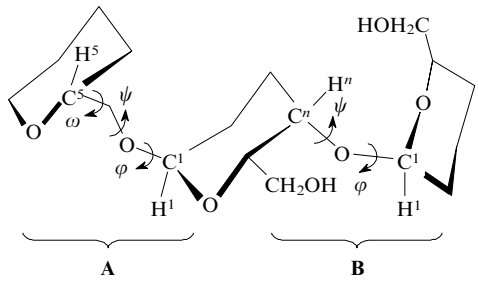
Received 10 April 2009
Uspekhi Khimii **78** (8) 776 – 795 (2009); translated by E E Yablonskaya

The activity of carbohydrate derivatives in biological processes is directly related to their spatial organization and, hence, the elucidation of factors regulating the conformational behaviour of oligo- and polysaccharides in solution is the topical task of modern physical chemistry of natural compounds. This area includes both theoretical studies of conformational properties, including their prediction, and experimental analysis of conformations of carbohydrate derivatives in solution. In our previous review,[19] we considered modern computation techniques in the theoretical studies of carbohydrate conformations. In the present review, we discuss the modern techniques of NMR spectroscopy for recording the proton – proton nuclear Overhauser effects (NOE), proton – proton and proton – carbon vicinal spin – spin coupling constants (SSCC) and the areas of their application in conformational analysis of carbohydrates in solution.

II. Structural and spectral (NMR) characteristics used in the conformational analysis of oligo- and polysaccharides

Numerous studies by various independent methods (X-ray crystallography, solution NMR spectroscopy, theoretical calculations) show that intraresidue bond lengths, bond and torsion angles of monosaccharides in the pyranose form depend slightly on the oligosaccharide type.[20] The pyranose residues in solution are characterized by one predominant conformation, either $^4C_1$ or $^1C_4$, depending on the monosaccharide nature. Unlike pyranoses, furanose rings are more flexible and exist in several interconverting conformations.[21–23]

The most important structural unit that determines the conformation of oligo- and polysaccharides is the intermonosaccharide bridge (Fig. 1), in which the bond lengths and bond angles vary insignificantly. The conformation mobility is provided by rotation about the bonds incorporated in the intermonosaccharide bridge.[20] For (1→6)-linked disaccharide units these are torsion angles φ, ψ and ω (fragment **A** in Fig. 1), whereas for (1→2)-, (1→3)- and (1→4)-linked



$n = 2-4$.

Figure 1. Torsion angles about the glycosidic bonds that determine the conformations of the (1→6)-linked disaccharide fragment (φ, ψ, ω) (fragment **A**) and the conformations of the (1→2)-, (1→3)- and (1→4)-linked disaccharide fragments (φ, ψ) (fragment **B**).

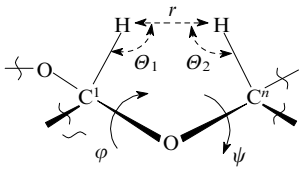


Figure 2. Interaction of the anomeric and transglycosidic protons in the intermonosaccharide bridge affecting the chemical shift values of signals for the C^1 and C^n carbon atoms linked through a glycosylated oxygen atom.

disaccharide units these are angles φ and ψ (fragment **B** in Fig. 1).

Among all the known experimental methods for the investigation of the structure of oligo- and polysaccharides in solution, ^1H and ^{13}C NMR spectroscopy is the most informative. Data on the structure can be obtained from proton nuclear Overhauser effect values,[24] from the values of spin–lattice relaxation time (T_1) of protons [24] and homo- and heteronuclear coupling constants between the ^1H and ^{13}C nuclei.[25–30]

The measured values of the NOE and relaxation times of protons are related to the direct dipole–dipole interaction of nuclei [31] and have the same physical nature. The spin–spin coupling constants reflect the indirect interaction of the nuclear spins transmitted through the polarization of valence electrons [32] and, thus, their physical nature differs from that of the NOE and relaxation times. Therefore, there are two independent approaches to the determination of structural parameters of oligo- and polysaccharides in solution using NMR spectroscopy.

It should be mentioned that information on carbohydrate structures can be obtained from the values of direct dipole–dipole constants observed in weakly oriented media. However, this approach will not be considered here, because the topic of the present review is restricted to the study of oligo- and polysaccharides in solutions. The studies of biomolecules in weakly oriented media are considered in another review.[33]

Indirect data on the conformations of disaccharide fragments of carbohydrates can be obtained from the values of ^{13}C nuclear chemical shifts in the close vicinity to the glycosidic bond. It was shown [34] that steric interactions of protons belonging to the neighbouring monosaccharide residues and localized at the glycosidic bond affect the chemical shifts of the carbon atoms bound to these protons (Fig. 2). The equation proposed [35] by Grant and Cheney in 1967 was used for the quantitative analysis of changes in chemical shifts in the ^{13}C NMR spectra.

$$\delta^{13}C = 1680\cos\Theta\exp(-2.671r), \quad (1)$$

where $\delta^{13}C$ is the chemical shift difference (ppm) due to the interaction of the neighbouring protons; r is the distance between the interacting protons (Å); Θ is the angle between the vectors C–H and H–H (see Fig. 2).

At present only the qualitative use of formula (1) is possible. Attempts of its quantitative application to the calculation of glycosylation effects or any other type of O-modification (O-sulfation, O-phosphorylation, *etc.*) for carbon atoms in oligo- and polysaccharides were unsuccessful. The reason is that the formula was obtained and parameterized for rough mechanical models of molecules, because in the 1960s the exact data on conformations of organic molecules were limited.

Carbohydrate molecules are characterized by several energy minima due to the flexibility of glycosidic bonds. Thus, it should be kept in mind that the experimentally observed characteristics of the NMR spectra are averaged over the ensemble of acceptable conformers. Therefore, the experimental data are usually analyzed considering the results of molecular modelling based on the molecular and quantum mechanics methods.

Indirect spin–spin interactions and the nuclear Overhauser effect are especially significant for studies of oligo- and polysaccharides in solution. In the next sections, we will consider their relationship to the structural parameters of molecules, the current experimental methods for their measurements and instantiate their application in structural analysis of carbohydrates.

III. Modern methods for the determination of spin–spin coupling constants and specific aspects of their use in conformational analysis of oligo- and polysaccharides

The homo- ($J_{H,H}$) and heteronuclear ($J_{C,H}$) SSCC find wide use in configurational and conformational analyses of carbohydrates. The vicinal (through three bonds) proton–proton SSCC ($^3J_{H,H}$) are used for the determination of the configuration of monosaccharide residues.

The dependence of the vicinal constants $^3J_{H,H}$ on the dihedral (torsion) angle H–C–C–H (θ) was experimentally found and theoretically substantiated. Karplus [36] pioneered in the theoretical prediction of this dependence in the form of equation (2), and modified equation (3) appeared later.[37]

$$^3J_{H,H} = A\cos^2\theta + B, \quad (2)$$

$$^3J_{H,H} = A\cos^2\theta + B\cos\theta + C. \quad (3)$$

The coefficients in Eqns (2) and (3) depend on the bond length between the carbon atoms (the $^3J_{H,H}$ constant is doubled with the shortening of the C–C bond from 1.46 to 1.34 Å), on the H–C–C bond angles (their decrease increases the constants) and on the electronegativity of substituents at the carbon atoms in the H–C–C–H fragment (the introduction of electronegative substituents decreases the $^3J_{H,H}$ constant).[25] It is especially difficult to take into account the influence of the latter factor, because

the $^3J_{H,H}$ value depends not only on the presence of electronegative substituents, but also on their arrangement relative to protons in the isomers or rotamers.

There were many attempts to write the Karplus equation in the explicit form for the H−C−C−H fragment with allowance for the listed factors.[38] Equation (4) proposed by Haasnoot *et al.*[39] seems to be the most successful attempt where the dependence of the constant value on not only the torsion angle θ but also the electronegativity of the first (α) and second (β) atoms in each substituent, as well as on the mutual orientation of these atoms, was taken into account.

$$^3J_{H,H} = P_1\cos^2\theta + P_2\cos\theta + \sum_i \Delta\chi_i[P_3 + P_4\cos^2(\xi_i\theta + P_5|\Delta\chi_i|)], \quad (4)$$

where P_1-P_5 are the parameters (Table 1) empirically found by least squares method from 315 experimental values of $^3J_{H,H}$;

$$\Delta\chi_i = \chi_i - \chi_H,$$

χ_i and χ_H are the electronegativities of the ith substituent and hydrogen, respectively; $\xi_i = \pm 1$ depending on the orientation of the ith substituent (Fig. 3). For the substituents containing the β-atoms,

$$\Delta\chi_i = \Delta\chi_i^{\alpha-\text{атом}} - P_6\sum_j \Delta\chi_j^{\beta-\text{атом}},$$

where P_6 is the parameter (see Table. 1).

Table 1. Dependence of the empirical parameters P_1-P_6 in Eqn (4) on the number of substituents S^i in the fragment H−C−C−H.

Parameter	1 substituent	2 substituents	3 substituents	4 substituents
P_1	13.70	13.89	13.22	13.24
P_2	−0.73	−0.98	−0.99	−0.91
P_3	0.56	1.02	0.87	0.53
P_4	−2.47	−3.40	−2.46	−2.41
P_5	16.9°	14.9°	19.9°	15.5°
P_6	0.14	0.24	0	0.19

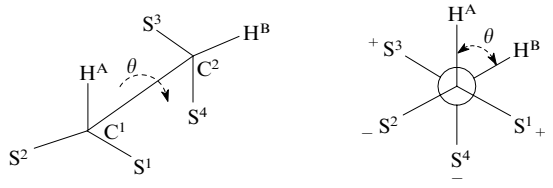


Figure 3. Determination of the 'positive' ($\xi_i = +1$) and 'negative' ($\xi_i = -1$) substituents S^i [for Eqn (4)] with respect to the H−C−C−H fragment of the tetrasubstituted ethane molecule.[39]

Equation (4) can also be used for the determination of the constants $^3J_{H,H}$ in carbohydrates. In practice, the inverse problem is often solved for these compounds: the torsion angles θ between two vicinal protons are determined from the experimental $^3J_{H,H}$ values using Eqn (4). As already mentioned, the monosaccharide residues in the pyranose form usually possess rigid conformations.[20] Therefore, from the experimental $^3J_{H,H}$ values between the intraresidue protons in the pyranose ring, one can readily calculate the corresponding torsion angles θ. In turn, from the angle values, one can determine the relative configurations of the chiral centres in the molecule and thus determine the type of the monosaccharide residue.

Depending on the mutual orientation of vicinal protons in the pyranose residues, three types of the coupling constants between them are distinguished (Fig. 4): $^3J_{a,a}$ is the coupling constant between two axial protons, $^3J_{e,a}$ is the coupling constant between the equatorial and axial protons

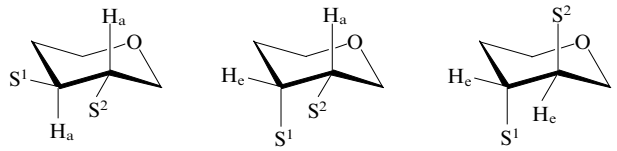


Figure 4. Types of coupling constants $^3J_{H,H}$ between the vicinal protons in the pyranose derivatives and the typical ranges of their values.

and $^3J_{e,e}$ is the coupling constant between the equatorial protons. The values of these constants vary in a relatively wide range (see Fig. 4) depending on the type of substituents S^1 and S^2 at the carbon atoms of the H−C−C−H fragment. However, in any pyranose residue the values of the coupling constants $^3J_{a,a}$ are larger and can easily be distinguished from the SSCC $^3J_{e,a}$ and $^3J_{e,e}$. The ranges of the coupling constants $^3J_{e,a}$ and $^3J_{e,e}$ overlap. Nevertheless, it was empirically found[26] that an individual set of coupling constants $^3J_{H,H}$ between the ring protons corresponds to each particular pyranose residue (Table 2). The exceptions are glycopyranose derivatives with conformationally flexible rings, namely, α-altrose, α- and β-idopyranoses, α- and β-ribopyranoses, α- and β-lyxopyranoses, including their analogues containing other functional groups (aminosaccharides, uronic acids and others). For the same reason, it is difficult to determine the configuration of furanose residues, where the presence of a bulky substituent at one of the hydroxy groups, including the anomeric group, can change

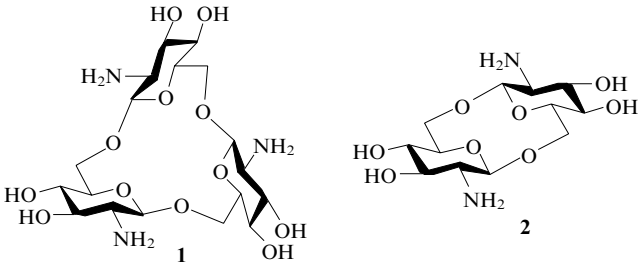
Table 2. Experimental values of coupling constants $^3J_{H,H}$ between the ring protons H^1-H^5 in the conformationally rigid pyranose rings.[26,27]

Configuration[a]	$^3J_{H^1,H^2}$ /Hz	$^3J_{H^2,H^3}$ /Hz	$^3J_{H^3,H^4}$ /Hz	$^3J_{H^4,H^5}$ /Hz
α-glc*p*	3.8	9.8	9.6	9.7
β-glc*p*	8.0	9.6	9.6	9.6
α-man*p*	1.5	3.3	9.6	9.6
β-man*p*	1.1	3.5	9.5	9.5
α-all*p*	3.8	3.3	3.1	9.6
β-all*p*	8.3	3.2	3.1	9.9
α-gal*p*	4.0	10.2	3.5	1.5
β-gal*p*	7.9	9.9	3.5	1.5
β-alt*p*	1.2	4.0	3.3	9.7
α-tal*p*	1.8	3.3	3.3	1.5
β-tal*p*	1.2	3.2	3.2	1.2
α-gul*p*	3.8	3.6	3.6	1.4
β-gul*p*	8.4	3.7	3.7	1.0

[a] Designations refer to the configuration of substituents in the pyranose rings and do not include the nature of substituents at C^5.

the predominant conformation of the ring compared to that for the unsubstituted residue [21–23] and, correspondingly, can change the $^3J_{H,H}$ coupling constant values between the ring protons.

It should be mentioned that strong steric hindrance in oligo- and polysaccharides can change even the conformations of stable pyranose rings. For example, the analysis of the experimental $^3J_{H,H}$ values for cyclic β-oligoglucosamines showed [40] that they changed strongly in disaccharide **2** as compared to trisaccharide **1**.



1 **2**

In the case of trisaccharide **1**, the coupling constants $^3J_{H,H}$ (Table 3) had values typical of the $^4C_1$ conformations of the β-glucopyranose residues (see Table 2). For disaccharide **2**, the $^3J_{H,H}$ values differed strongly from the typical values, indicating strong distortion of the $^4C_1$ conformations of the pyranose rings. The change in the conformations of the glucopyranose residues in the disaccharide favours the release of the steric strain that occurs in this molecule.

The $^3J_{H,H}$ values can be determined from the multiplicities of the signals in the 1D ^{1}H NMR spectrum. However, for higher oligosaccharides and polysaccharides with the repeating units built of many monosaccharide residues, the determination of the $^3J_{H,H}$ values from these spectra is often impossible because of strong overlap of the signals. In this case, phase-sensitive ^{1}H–^{1}H COSY,[41–43] COSY-DQF,[43,44] E.COSY,[43,45,46] PE.COSY [43,47] and heteronuclear ^{1}H–^{13}C HMQC,[48] HSQC,[49] XLOC [50–52] 2D experiments are usually employed (the description of these experiments is given below). The application of these methods makes it possible to present the data of the 1D ^{1}H NMR spectrum in two dimensions; as a result, the number of overlapped signals decreases strongly and the measurement of the $^3J_{H,H}$ constants becomes possible.

Another type of constants that are often used for the determination of monosaccharide configurations is direct proton–carbon coupling constants ($^1J_{C,H}$). Analysis of the coupling constants between the C^1 and H^1 atoms ($^1J_{C^1,H^1}$) in monosaccharide residues makes it possible to exactly distinguish the furanose and pyranose forms of molecules: for the monosaccharide residues in the furanose form they are 173–175 Hz regardless of the configuration of the anomeric centre (α or β), in the pyranose residues with the α-configuration of the anomeric centre these values range from 168 to 173 Hz, whereas for the β-configuration they are 155–165 Hz. The GATED,[32] HMQC [48,53] and HSQC [49,53] experiments (see below) are usually employed to determine the coupling constants $^1J_{C,H}$.

From the technical viewpoint, the simplest experiment providing information about the coupling constants $J_{C,H}$ is recording of the ^{13}C NMR spectrum without suppression of carbon–proton spin–spin interactions (without 'proton decoupling'). In this case, one should take into account that ^{13}C NMR spectroscopy is considerably less sensitive than ^{1}H NMR spectroscopy because of the low content of the ^{13}C isotope in the sample (the natural abundance is 1.1%) and the lower magnetization of the ^{13}C nuclei [the gyromagnetic ratio of the ^{1}H nucleus (γ_H) exceeds that of ^{13}C nucleus (γ_C) by a factor of 3.97]. To obtain ^{13}C NMR spectra with the high signal-to-noise ratio, the free induction decay (FID) acquisition should be run for a long time.

The sensitivity of the ^{13}C NMR experiment can be enhanced owing to the nuclear Overhauser effect emerging on the ^{13}C nuclei with the saturation of transitions of the ^{1}H nuclei.[32] For this purpose, the broad band (BB mode) low-power radiofrequency irradiation of the whole range of ^{1}H nuclear resonances in the molecule is performed during the relaxation delay. This is the so-called GATED experiment (Fig. 5).

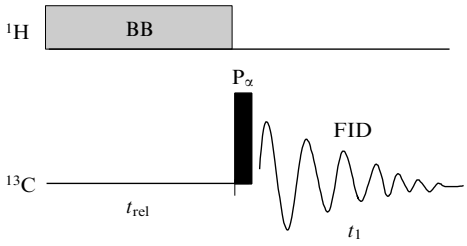
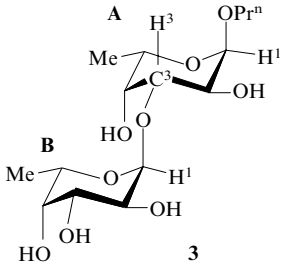


Figure 5. Pulse sequence in the GATED experiment.
P_α is the excitation electromagnetic pulse at the frequency of the ^{13}C nuclei generated by the spectrometer transmitter; BB is the broad-band low-power radiofrequency irradiation acting on the whole ^{1}H nuclear range; t_{rel} is the relaxation delay; FID is the free induction decay detected by the spectrometer receiver within the t_1.[32]

Figure 6*b* presents the GATED spectrum of propyl (1→3)-fucosyl-fucoside (**3**) recorded by us.



3

In this spectrum, the signals corresponding to particular carbon atoms are split into multiplets due to C–H cou-

Table 3. Experimental values of the coupling constants $J_{H,H}$ for cyclic tri- and diglucosamines inferred from the ^{1}H NMR spectra (spectrometer 500 MHz, D_2O, 303 K).[40]

Compound	$^3J_{H^1,H^2}$ /Hz	$^3J_{H^2,H^3}$ /Hz	$^3J_{H^3,H^4}$ /Hz	$^3J_{H^4,H^5}$ /Hz	$^3J_{H^5,H^{6R}}$ /Hz	$^3J_{H^5,H^{6S}}$ /Hz	$^2J_{H^{6R},H^{6S}}$ /Hz
[-β-(1→6)-GlcNH$_2$-]$_3$ (**1**)	8.1	8.9	9.1	9.1	3.9	~1	12.2
[-β-(1→6)-GlcNH$_2$-]$_2$ (**2**)	⩽1	5.7	9.8	9.8	1.9	⩽1	12.8

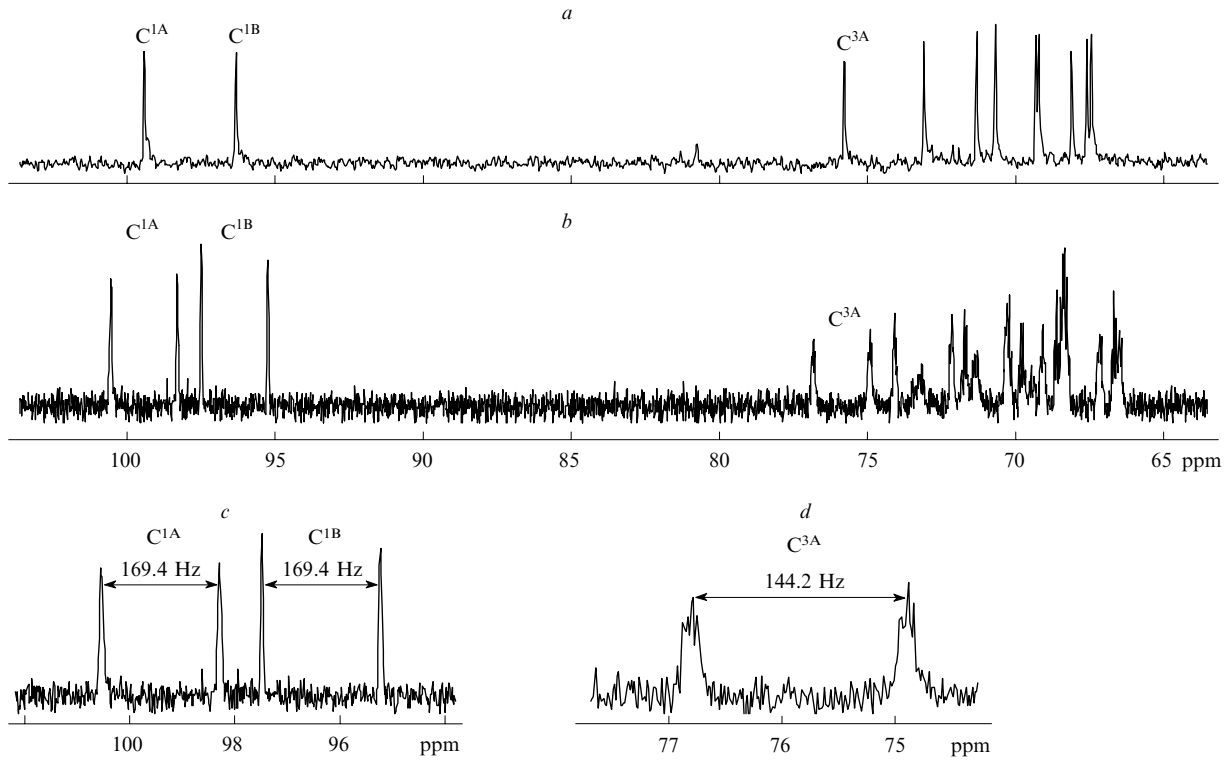
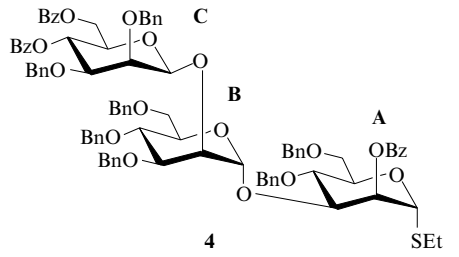


Figure 6. The ^{13}C NMR spectra of propyl (1→3)-fucobioside (**3**) (500 MHz spectrometer, D_2O, 303 K). (*a*) Spectrum with the broad-band proton decoupling; (*b*) GATED spectrum; (*c*) fragment of the GATED spectrum containing signals of the carbon atoms C^{1A} and C^{1B} split due to the SSCC $^1J_{C^1,H^1}$ (169.4 Hz); (*d*) fragment of the GATED spectrum containing the signal of the carbon atom C^{3A}.

pling, revealing both the direct ($^1J_{C,H}$) and long-range coupling constants ($^2J_{C,H}$, $^3J_{C,H}$). This spectrum made it possible to determine the values of the $^1J_{C^1,H^1}$ constants between the anomeric C^1 and H^1 atoms in monosaccharide residues **A** and **B**, which were equal to 169.4 Hz (Fig. 6 *c*). Thus, it was unambiguously shown that residues **A** and **B** in the disaccharide under study had the α-configuration. Note that in the GATED spectrum the long-range coupling constants $^2J_{C,H}$, $^3J_{C,H}$ for the C^1 atoms of this compound are not resolved because of their too low values. The spectrum also allows one to determine the $^1J_{C^3,H^3}$ value (144.2 Hz). However, it is difficult to find the $^3J_{C,H}$ values because of the high noise level in the spectrum (Fig. 6 *d*).

A drawback of the GATED experiment in $J_{C,H}$ constant determination is that the spectrum is difficult to interpret. As a rule, each carbon atom in the molecule is spin–spin coupled to several (N) protons and, hence, its signal is split into 2^N components. The structure of oligo- and polysaccharides contains large groups (tens and even hundreds) of non-equivalent carbon atoms, each having several lines (due to splittings) in the GATED spectrum, due to which the latter are difficult to interpret without additional experiments. Therefore, in the case of higher oligosaccharides and polysaccharides, HMQC (Heteronuclear Multiple Quantum Coherence)[48,53] and HSQC (Heteronuclear Single Quantum Coherence) 2D experiments (NMR methods based on the excitation and detection of heteronuclear multiple quantum or single quantum coherence, respectively) are usually employed for the determination of direct coupling constants $^1J_{C,H}$.[49,53] Unlike the GATED spectra, in 2D HMQC and HSQC spectra recorded in the decoupling mode, the chemical shifts of the ^{13}C nuclei and $^1J_{C,H}$ constants are plotted alongside different dimensions (F1 and F2, respectively).

Figure 7 shows the fragment of the HSQC spectrum of synthetic trimannoside **4** containing the correlation peaks corresponding to the interaction of the carbon C^1 atoms and protons H^1 (Ref. 54).



4

The spectrum was recorded in the decoupling mode and made it possible to determine the coupling constants $^1J_{C^1,H^1}$ for mannopyranose residues **A**, **B** and **C** that were equal to 168, 170 and 155 Hz, respectively. For residues **A** and **B**, $^1J_{C^1,H^1} \geqslant 168$ Hz, and for residue **C** $^1J_{C^1,H^1} < 165$ Hz. Thus, it was unambiguously established that residues **A** and **B** have the α-configuration and residue **C** is in the β-configuration. Note that it is impossible to determine the anomeric configuration of these mannopyranose residues from the vicinal proton–proton constants ($^3J_{H^1,H^2}$) because of overlap of the acceptable ranges for $J_{a,e}$ and $J_{e,e}$ (see Fig. 4).

The difference between the HMQC and HSQC spectra is only that the correlation peaks in the former are split along

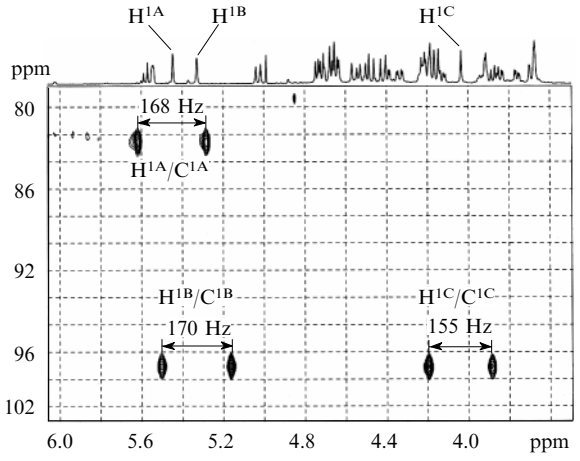


Figure 7. A fragment of the HSQC spectrum (recorded without decoupling, 500 MHz spectrometer, $CDCl_3$, 303 K) of synthetic trimannoside **4**.[54]
The region of interaction of the C^1 carbon atoms and H^1 protons is shown.

the vertical axis (F1 dimension) due to the proton–proton SSCC ($J_{H,H}$) and, hence, their shape is broader along this dimension. As a result, the HMQC spectrum is somewhat less resolved along the F1 axis than the HSQC spectrum. However, the pulse sequence of the HMQC experiment contains smaller number of pulses and instrumental delays and therefore is simpler and less sensitive to the instrument adjustments.

Let us consider the pulse sequence in the 2D HMQC experiment (Fig. 8). First, a non-selective 90° pulse (P_{90}) at the frequency of protons acts on the system and transfers the magnetization vectors (Fig. 9) to the plane *xy*. Then the evolution of the system occurs during the time interval Δ under the action of chemical shifts of the ^1H nuclei and SSCC (both homonuclear, $J_{H,H}$ and heteronuclear, $J_{C,H}$). The delay duration Δ is selected such that the magnetizations caused by the direct coupling constants $^1J_{C,H}$ are in antiphase: $\Delta = 1/(2\ ^1J_{C,H})$. In the HMQC experiment, Δ is usually specified as 3.3 ms, which corresponds to the average value of the coupling constant $^1J_{C,H}$ in organic molecules equal to 150 Hz. This is prerequisite for the subsequent generation of heteronuclear multiple quantum coherence by the 90° pulse at the frequency of the ^{13}C nuclei (see Fig. 8), which transfers the magnetization vectors of the ^{13}C nuclei also to the plane *xy*.

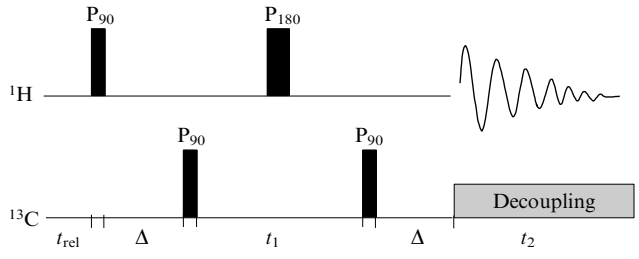


Figure 8. Pulse sequence in a 2D HMQC experiment (see text).

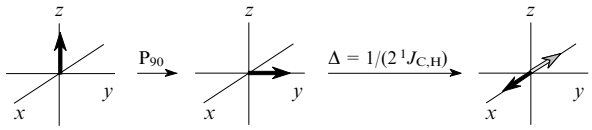


Figure 9. Evolution of the ^1H nuclear magnetization in the first stage of the HMQC experiment.
The delay duration Δ is selected in such a way as to provide the antiphase arrangement of proton magnetizations caused by the SSCC $^1J_{C,H}$, which is necessary for the further development of the multiple quantum coherence.

The heteronuclear multiple quantum coherence is characterized by the state of the system where the magnetizations of the nuclei of both types (^1H and ^{13}C) are in the transverse plane.[53] It is of interest to follow the development of the multiple quantum coherence during the evolution time t_1, but it is impossible to correctly describe this coherence in terms of the vector model. It is known that the heteronuclear multiple quantum coherence develops under the action of chemical shifts of both protons and ^{13}C nuclei. However, its specific feature is that the coherence does not develop under the action of the 'active' coupling constants $^1J_{C,H}$. Remind that the 2D HMQC spectrum in the F1 dimension contains no information on chemical shifts of ^1H nuclei, which is achieved by refocusing their magnetization formed during the evolution period t_1 through the 180° pulse at the proton frequency in the middle of the period t_1 (spin echo creation). This pulse exerts no effect on the evolution of chemical shifts of ^{13}C nuclei and therefore the ^{13}C chemical shifts provide the frequency marking of the F1 dimension of the 2D spectrum. At the end of the period t_1, the system is affected by the final 90° pulse at the frequency of the carbon nuclei. This pulse withdraws the magnetizations from the plane *xy*, whereas the magnetizations of protons remain in this plane. The proton magnetizations coupled to each other by $^1J_{C,H}$ occur again in the antiphase. The second delay Δ (its duration is equal to the first delay Δ) is inserted into the end of the pulse HMQC sequence in order to re-focus these magnetizations. After the second delay, the proton magnetizations are detected as the FID during the time t_2. The result of the double Fourier transform of the obtained data set is the 2D HMQC spectrum in which the correlations appear between the ^1H and ^{13}C atoms coupled by the direct SSCC $^1J_{C,H}$. The correlation signals along the proton axis (F2 dimension) are split into doublets with the couplings equal to those of $^1J_{C,H}$ (see Fig. 7). If information about the $^1J_{C,H}$ values is redundant, the 2D HMQC experiment is carried out in the decoupling mode, which makes it possible to enhance the sensitivity of the experiment due to merging the components of the multiplet signals into singlets. In this case, the ^{13}C nuclei of the system are subjected to the broad band irradiation with the electromagnetic field generated by the spectrometer transmitter during the detection of the FID from the protons (see Fig. 8). Note that it is the decoupled 2D HMQC spectra that are used for the determination of the homonuclear $J_{H,H}$ values.

The second delay Δ at the end of the HMQC pulse sequence (see Fig. 8) also allows one to re-focus the influence of shifts of the ^1H nuclei that exists during the first delay Δ (in the beginning of the HMQC pulse sequence). Remind that during the first delay Δ the evolution of the

system occurs due not only to the direct $^1J_{C,H}$ constants discussed, but also chemical shifts of the ^1H nuclei and homonuclear $J_{H,H}$ constants. However, the influence of the $J_{H,H}$ constants on the ^1H nuclear magnetization cannot be eliminated and, hence, the correlation peaks in the HMQC spectrum are split due to $J_{H,H}$ along the F1 axis. As already said, this splitting is absent from the HSQC spectra, which are consequently better resolved in the F1 dimension.

The main problem of the HMQC experiment is the suppression of the $^1H-^{12}C$ signals, which can hide the desirable correlation peaks caused by the constants $^1J_{C,H}$. The application of new methods of gradient spectroscopy [55, 56] made it possible to carry out an efficient suppression of unnecessary magnetization components (coherences) during pulse sequences of NMR experiments. For example, the use of pulse field gradients in the HMQC experiment allows one to completely annihilate the $^1H-^{12}C$ signals.[53]

Yet another type of SSCC that are often used in structural analysis of oligo- and polysaccharides, are the vicinal proton–carbon coupling constants ($^3J_{C,H}$). As already said, conformations of disaccharide fragments are primarily defined by values of torsion angles φ and ψ at the glycosidic bonds (see Fig. 1). The vicinal SSCC can be put in correspondence to each angle: the J_φ constant in the fragment $^{13}C^n-O-C^1-H^1$ corresponds to the angle φ, and the J_ψ constant in the fragment $^{13}C^1-O-C^n-H^n$ corresponds to the angle ψ.

The angular Karplus dependence is versatile for all magnetic nuclei and, in particular, for the spin–spin coupling of the ^{13}C nucleus and proton through three bonds in the fragments $^{13}C-X-Y-^1H$, where X and Y are any atoms.[57] As we have already seen, the coupling constants $^3J_{C,H}$ through the oxygen atom in the fragment $^{13}C-O-C-^1H$ are most important for structural chemistry of oligo- and polysaccharides. By comparing the coupling constants $^3J_{C,H}$ for various carbohydrates in which the $^{13}C-O-C-^1H$ fragments exist in one preferential conformation and the torsion angle values in the crystal structures of these molecules determined by X-ray diffraction analysis, the Karplus equation (5) for this fragment was obtained [28] (Fig. 10).

$$J_\theta = 5.5\cos^2\theta - 0.7\cos\theta + 0.6, \qquad (5)$$

where $\theta = \varphi$ or ψ, $J_\theta = J_\varphi$ or J_ψ.

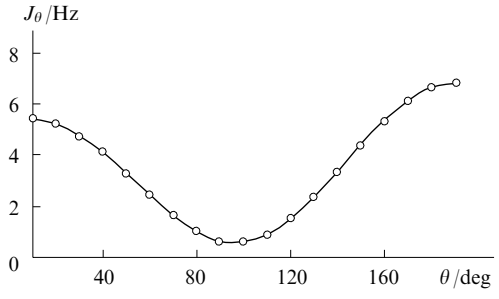


Figure 10. Dependence of the coupling constant J_θ on the dihedral angle of the $^{13}C-O-C-^1H$ fragment in carbohydrates [see Eqn (5)].[28]

Thus, with the experimental values of the J_φ and J_ψ constants at hand and using Eqn (5), one can calculate the values of torsion angles φ and ψ at the glycosidic bonds, which provides a possibility of conformational analysis of oligo- and polysaccharides. It should be kept in mind that the observed J_φ and J_ψ constant values are averaged over an ensemble of acceptable conformers of the glycosidic bond. Also note that other equations similar to Eqn (5) were obtained [29, 30] for the $^{13}C-O-C-^1H$ fragment of carbohydrates.

In the case of (1→6)-linked disaccharide fragments (see Figs 1 and 11), the J_φ and J_ψ constants described by Eqn (5) correspond to the angles φ and ψ, and the heteronuclear constants $^3J_{H^{6R},C^4}$ and $^3J_{H^{6S},C^4}$ [Eqn (6) [58]] or homonuclear constant $^3J_{H^{6R},H^5}$ and $^3J_{H^{6S},H^5}$ [Eqns (4) or (7), (8) [59]] can be put in correspondence to the angle ω; Eqns (7) and (8) are specially adapted for the calculation of the coupling constants $^3J_{H,H}$ corresponding to the hyroxymethyl group of the hexopyranose residues.

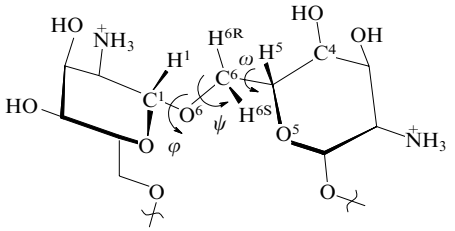
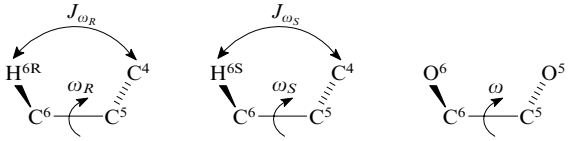


Figure 11. Torsion angles φ, ψ and ω in the di-β-(1→6)-glucosamine fragment, which is the major structural unit of poly(*N*-acetylglucosamine). The latter is the extracellular polysaccharide (adhesin) produced by *Staphylococcus aureus* and a number of other bacteria.[14]



$$J_{\omega'} = 8.06\cos^2\omega' - 0.87\cos\omega' + 0.47,\ \omega' = \omega_R \text{ or } \omega_S, \qquad (6)$$

$$^3J_{H^{6R},H^5} = 5.08 + 0.47\cos\omega + 0.90\sin\omega - 0.12\cos(2\omega) + 4.86\sin(2\omega), \qquad (7)$$

$$^3J_{H^{6S},H^5} = 4.92 - 1.29\cos\omega + 0.05\sin\omega + 4.58\cos(2\omega) + 0.07\sin(2\omega). \qquad (8)$$

Note that the functions corresponding to Eqns (5)–(8) are periodical and hence several values of torsion angles may correspond to one experimental value of the coupling constant J. The wrong angle values can usually be excluded on the basis of the theoretical conformational analysis.

As already mentioned, the $^3J_{H,H}$ values are usually easy to determine. The GATED,[32] HMBC,[51, 60–63] HSQMBC [64, 65] NMR experiments, 2D J spectroscopy [66, 67] and experiments of the E.COSY type,[45, 46] namely, X-filtred NOESY, TOCSY and RELAY COSY,[68–70] can be used for the determination of $^3J_{C,H}$ values. Let us consider in more details the principles of these experimental protocols.

We will discuss their advantages and disadvantages and consider specific examples of their application for the determination of the SSCC $^3J_{C,H}$.

The GATED spectrum contains information on the direct coupling constants $^1J_{C,H}$ and also the long-range constants $^nJ_{C,H}$ (where $n \geqslant 2$). Figure 6 *d* shows the fragment of the GATED spectrum of (1→3)-fucobioside containing the signal of the glycosylated carbon atom C^{3A}. This signal is split into a multiplet due to the spin–spin coupling of this carbon atom with the protons H^{3A} ($^1J_{C,H}$), H^{1A} ($^3J_{C,H}$) and H^{1B} ($^3J_{C,H}$) of the glycosylating residue. The large coupling constant through one bond between the C^{3A} carbon atom and H^{3A} proton ($^1J_{C,H}$ = 144.2 Hz) is well determined in this GATED spectrum. However, it is impossible to exactly determine small coupling constants through three bonds ($^3J_{C,H}$) because of the high noise level in the spectrum.

Information on the long-range coupling constants $^nJ_{C,H}$ can also be obtained from experiments of the HMBC (Heteronuclear Multiple-Bond Correlation) type, which make it possible to reveal heteronuclear correlations through several bonds.[53, 71] The ^{1}H and ^{13}C chemical shifts are plotted on the F2 and F1 axes in the 2D HMBC spectrum, respectively (Fig. 12), whereas the correlations in the spectrum lie on the intersection of the coordinates corresponding to the chemical shifts of the nuclei that are bound by the long-range SSCC. The HMBC experiment seems to be most convenient for the determination of the heteronuclear spin–spin interactions, because it contains information on all interactions of this kind that occur in the molecule. Unlike the GATED spectrum, the data in the HMBC spectrum are presented in two dimensions, which decreases the probability of signal overlap.

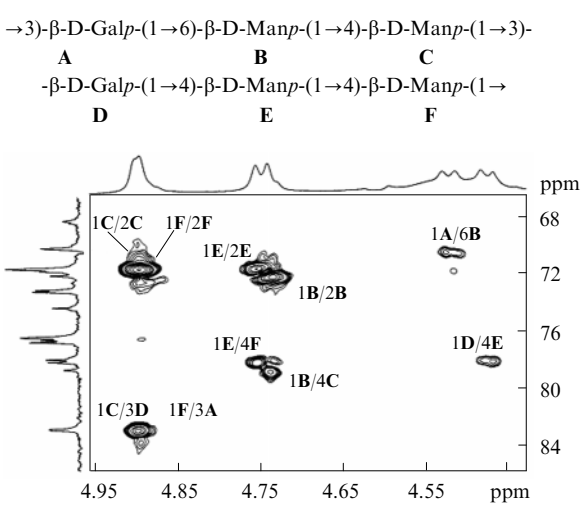


Figure 12. A fragment of the $^1H-^{13}C$ HMBC spectrum (500 MHz spectrometer, D_2O) of polysaccharide from the cell wall of the actinomycete *Kineosporia aurantiaca* VKM Ac-702^T (see Ref. 72).
The correlation signals in the spectrum reflect the interactions of the anomeric protons of polysaccharide characterized by the long-range coupling constants $^nJ_{C,H}$. The digits before and after the slash refer to the H and ^{13}C atoms, respectively, of the residues **A**–**F**.

The pulse sequence of the 2D HMBC experiment (Fig. 13) is similar to that of the 2D HMQC experiment (see Fig. 8), except for two points. First, the delay duration (Δ) in the HMBC experiment is substantially longer. This

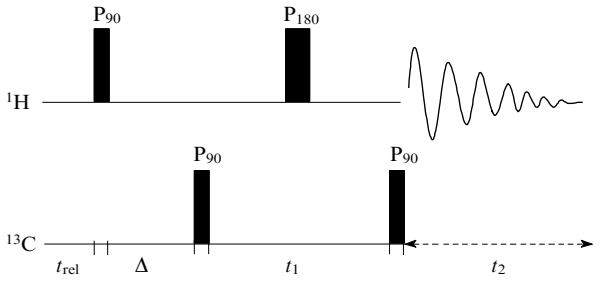


Figure 13. Pulse sequence in a 2D HMBC experiment (see text).

duration is selected such that the antiphase arrangement of magnetizations caused by small long-range coupling constants $^nJ_{C,H}$ is formed. As a rule, $^nJ_{C,H} < 8$ Hz and, therefore, the delay Δ should be at least 60 ms ($1/2\ ^nJ_{C,H}$).[53] Second, to decrease the sensitivity loss in the HMBC experiment due to relaxation processes, the end of its pulse sequence should contain no second re-focusing delay Δ. This results in the distorting of the signal phase and, hence, the HMBC spectra are usually presented as a phase-insensitive power spectrum. Although the delay Δ is chosen on the basis of the long-range SSCC values, sometimes the delays that characterize the direct interactions ($1/2\ ^1J_{C,H}$) are proportional to Δ. In these cases, the correlations caused by the direct coupling constants $^1J_{C,H}$ also appear in the spectrum. However, they are split into doublets along the F2 axis, because the FID of protons is detected in the HMBC experiment without decoupling from ^{13}C nuclei. The direct constants $^1J_{C,H}$ can be suppressed by low-pass J-filter (LPJF),[73] which quenches modulations generated by the SSCC having frequencies higher than the specified frequency (in our cases, this is a frequency of 125 Hz, because for organic molecules $^1J_{C,H} \geqslant 125$ Hz). Depending on the required filtration band, the LPJF with the number of steps from 1 to 3 are used.

The HMBC spectrum provides information on the protons and ^{13}C nuclei bound by the long-range coupling constants $^nJ_{C,H}$. However, this spectrum contains no information about the values of these constants. The experiments that make it possible to determine the values of long-range coupling constants $^nJ_{C,H}$ were developed on the basis of the HMBC pulse sequence. One of such experiments is 2D J-HMBC.[51, 61] The 2D J-HMBC spectrum (Fig. 14) has the same format as the standard 2D HMBC spectrum, except for the fact that the correlation peaks caused by the long-range interactions in the 2D J-HMBC spectrum are split into doublets along the ^{13}C axis (F1 dimension). The splittings are proportional to the long-range $^nJ_{C,H}$ values that cause the occurrence of these correlations. The scale factor *k* defining the splitting value of the peaks depends on the experimental conditions and is expressed as follows:

$$k = \frac{\Delta}{t_1^{\max}},$$

where $t_1^{\max}$ is the maximum duration of the evolution period t_1 (Fig. 15). The Δ value should correspond to the lowest value of the long-range coupling constant $^nJ_{C,H}^{\min}$, which should precisely be measured, *i.e.*,

$$\Delta = \frac{1}{2\ ^nJ_{C,H}^{\min}}.$$

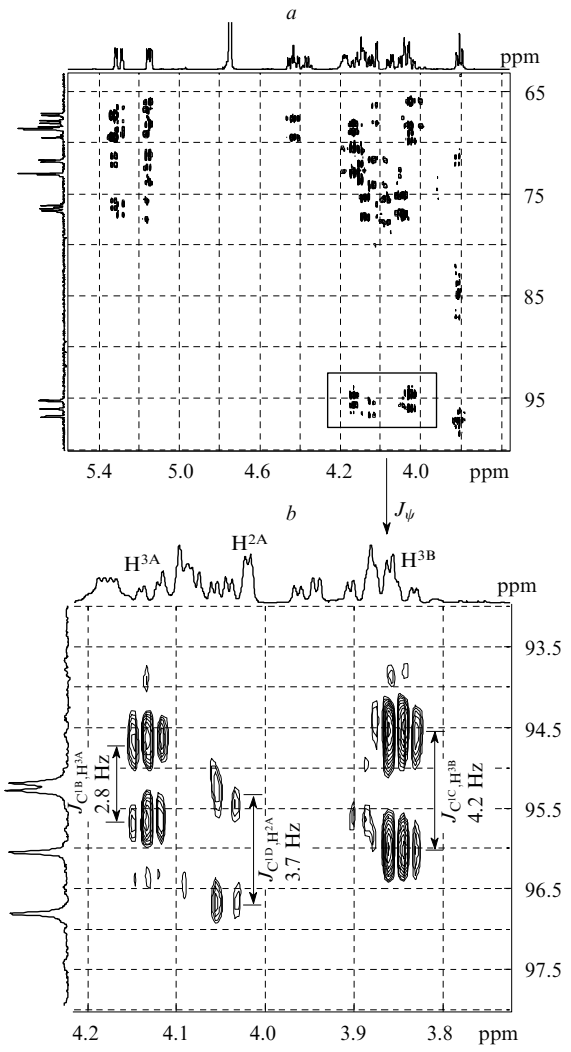


Figure 14. Application of the 2D J-HMBC experiment for the determination of the long-range coupling constants $^nJ_{C,H}$ (see Ref. 74). (*a*) J-HMBC spectrum of sulfated tetrafucoside **5** (500 MHz spectrometer, D_2O, 303 K). In this spectrum, the correlations are split along the ^{13}C axis into doublets (scaling coefficient $k = 34$); (*b*) a fragment of the J-HMBC spectrum of tetrafucoside **5** that made it possible to determine the coupling constants J_ψ for three glycosidic bonds of the molecule.

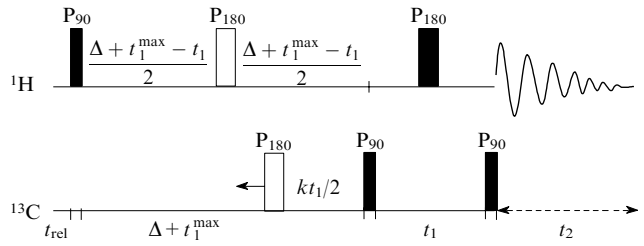


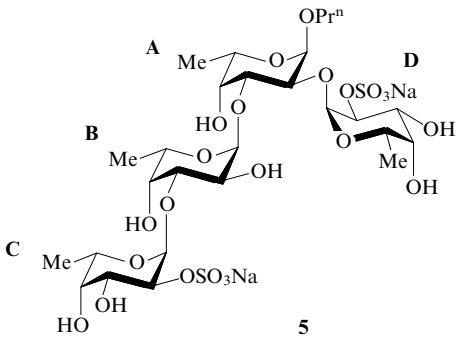
Figure 15. Pulse sequence in a 2D J-HMBC experiment (see text).[51, 61]

The 2D J-HMBC spectrum of sulfated tetrafucoside **5** presented in Fig. 14 made it possible to determine the values of the majority of transglycosidic constants J_φ and J_ψ in the molecule (Table 4).[74]

Table 4. Experimental (500 MHz spectrometer, D_2O, 303 K) [a] and calculated values of the transglycosidic coupling constants J_φ and J_ψ for sulfated tetrafucoside **5**.[74]

Disaccharide fragment	J_φ /Hz		J_ψ /Hz	
	experiment	calculation	experiment	calculation
→3)-α-L-Fuc-(1→3)-α-L-Fuc-OPr^n	4.4 [b]	3.5	2.8	3.0
→3)-α-L-Fuc-(1→3)-α-L-Fuc-(1→	3.7	3.4	4.2	3.7
α-L-Fuc-(1→2)-α-L-Fuc-OPr^n	2.3	2.7	3.7	3.3

[a] Most constants were determined from the 2D J-HMBC spectrum (Fig. 14). [b] The constant was determined from the 2D *J* spectrum (for its description, see further). This value cannot be determined from the 2D J-HMBC spectrum because of signal overlap.



The theoretical conformational analysis by molecular mechanics (MM3 force field) for this compound [74] showed two conformers for the (1→3)-bonds and one conformer for the (1→2)-bond. The averaged constants were calculated on the basis of the theoretical simulation (see Table 4). A comparison of the experimental and calculated J_φ and J_ψ values shows good agreement (the discrepancy does not exceed 1 Hz), indicating that the theoretical conformational analysis data are reliable. Thus, the combined analysis of the experimental and theoretical data made it possible to determine the conformational characteristics of tetrafucoside **5**.

The pulse duration of the 2D J-HMBC experiment (see Fig. 15) differs from that of 2D HMBC (see Fig. 13) by additional 180° pulses at the frequencies of the protons and ^{13}C nuclei, which act during the delay Δ. The moments of their application change proportionally to the change in the period t_1 during the 2D experiment. In order to distinguish the desirable magnetizations and to eliminate the magnetizations caused by the non-ideal character of the 90° and 180° pulses, the 2D J-HMBC experiment is carried out using the pulse gradients of the field $\mathbf{B}_0$.[51, 55]

Other procedures for measuring long-range coupling constants $^nJ_{C,H}$ [60, 62, 63] based on the HMBC sequence and similar to the J-HMBC experiment [51, 61] are also documented. However, these procedures are less convenient in practice or require additional calculations to obtain necessary information on the constants. Looking ahead, we can mention that the J-HMBC experiment is the most convenient and versatile, in our opinion, among all presently known methods for the determination of long-range coupling constants $^nJ_{C,H}$.

The 2D HSQMBC (Heteronuclear Single Quantum Multiple-Bond Correlation)[64,65] spectrum (Fig. 16 *a*) has the same format as the 2D HMBC spectrum. In this spectrum, the ^{1}H and ^{13}C chemical shifts are plotted on the axes F2 and F1, respectively, and the correlation peaks in the spectrum correspond to the nuclear pairs $^{1}H/^{13}C$ bound by the long-range coupling constants $^{n}J_{C,H}$. The spectrum contains information on all long-range spin–spin $^{13}C/^{1}H$ interactions that occur in the molecule. However, the full line shape of the correlations should necessarily be analyzed to determine the $^{n}J_{C,H}$ values from the 2D HSQMBC spectrum, Figure 16 demonstrates the determination of the constants $^{3}J_{C^{2A},H^{1B}}$ and $^{2}J_{C^{1B},H^{2B}}$ in sucrose.[64] For this purpose, the shape of the correlation peaks corresponding to these constants was simultated from the 2D HSQMBC spectrum using one-dimensional proton spectra or from the 2D HSQC spectrum using the cross sections. In the 2D HSQMBC spectrum, the correlation C^{i}/H^{j} (between the *i*th carbon atom and *j*th proton coupled by the long-range constant $^{n}J_{C^{i},H^{j}}$) along the proton axis (F2 axis) is split into a multiplet due to the long-range coupling constant $^{n}J_{C^{i},H^{j}}$ and due to the proton–proton coupling constants $J_{H^{j},H^{k}}$ that characterize the proton H^{j}. The constant $J_{C^{i},H^{j}}$ determines the antiphase arrangement of signals in the multiplet, and the constant $J_{H^{j},H^{k}}$ determines the synphase arrangement. This multiplet can be simulated from the corresponding signal of the proton spectrum. For this purpose, two ^{1}H NMR spectra (one of which is in the antiphase) shifted relative to each other by the value of the coupling constant $J_{C,^{i},H^{j}}$ should be summated. Thus, to determine the constant $J_{C^{i},H^{j}}$ by the 2D HSQMBC procedure, the section of the correlation C^{i}/H^{j} should be simultated by two proton spectra. The shift value of one ^{1}H NMR spectrum relative to another is equal to the constant $J_{C^{i},H^{j}}$.

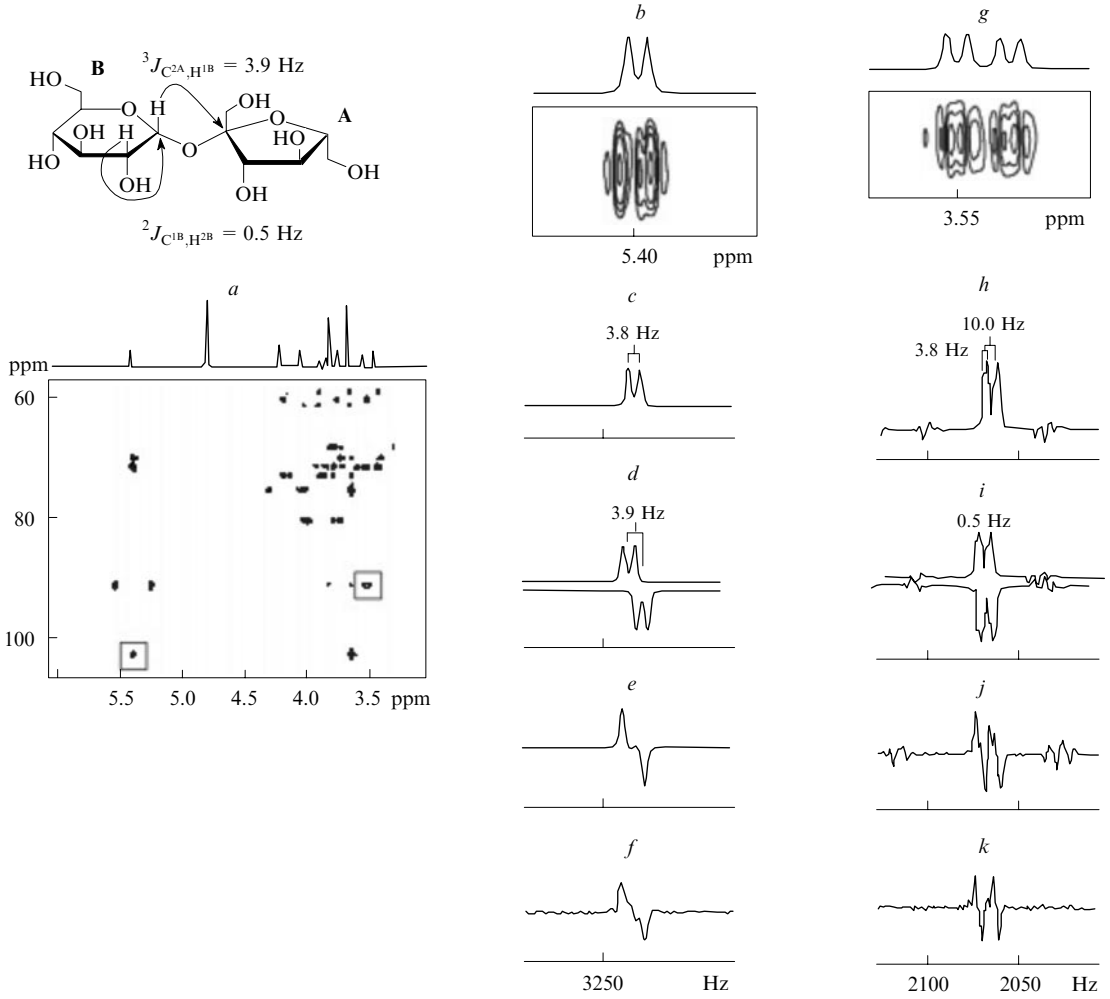


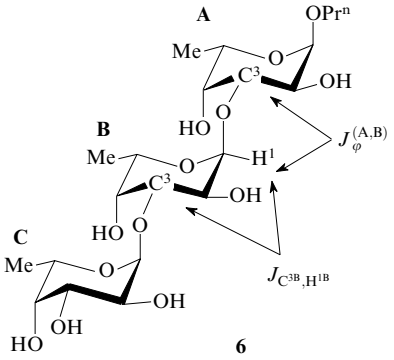
Figure 16. A procedure for determination of the long-range coupling constants $^{n}J_{C,H}$ from the 2D HSQMBC spectrum.[64]
(*a*) 2D HSQMBC spectrum of sucrose (600 MHz spectrometer, D_2O);[65] (*b*) a fragment of the 2D HSQMBC spectrum that reflects the interaction of the atoms C^{2A} and H^{1B}; (*c*) a fragment of the ^{1}H NMR spectrum containing the signal for H^{1B}; (*d*) two signals for H^{1B} in the antiphase shifted relative to each other by the heteronuclear coupling constant $J_{C^{2A},H^{1B}}$ of 3.9 Hz; (*e*) the result of summation of two doublets shifted relative to each other presented in Fig. *d*; (*f*) a horizontal section of the correlation C^{2A}/H^{1B} from the 2D HSQMBC spectrum; (*g*) a fragment of the 2D HSQMBC spectrum that reflects the interaction of the atoms C^{1B} and H^{2B}; (*h*) a section from the 2D HSQC spectrum containing the signal for H^{2B}; (*i*) two signals for H^{2B} in the antiphase shifted relative to each other by the heteronuclear coupling constant $J_{C^{1B},H^{2B}}$ of 0.5 Hz; (*j*) the result of summation of two signals for H^{2B} shifted relative to each other of presented in Fig. *i*; (*k*) a horizontal section of the C^{1B}/H^{2B} correlation from the 2D HSQMBC spectrum.

Since the additional analysis of the signal line shape is necessary, the 2D HSQMBC experiment is less convenient for the determination of the long-range coupling constants $^{n}J_{C,H}$ than the 2D J-HMBC experiment. However, the 2D HSQMBC experiment can be useful when the constants cannot be determined by the 2D J-HMBC experiment because of the overlap of the correlation peaks in the spectrum. Remind that in the 2D J-HMBC spectrum the long-range $^{n}J_{C,H}$ coupling constants appear as the splitting of the correlation peaks along the ^{13}C axis (F1 dimension) and, therefore, this spectrum is less resolved along the ^{13}C axis than the 2D HSQMBC spectrum in which the constants are observed along the ^{1}H axis. Another significant advantage of the 2D HSQMBC experiment is that the values $J_{C,H} < 2$ Hz can be determined rather accurately from this experiment, which is difficult to do from the 2D J-HMBC experimental data. As shown in Fig. 16, the value of the coupling constant $^{2}J_{C^{1B},H^{2B}}$ of 0.5 Hz was determined for sucrose using the 2D HSQMBC experiment. For the precise determination of this constant by the 2D J-HMBC experiment, one should use the delay

$$\Delta = \frac{1}{2\,{}^{n}J^{\min}_{C,H}} = \frac{1}{2J_{C^1,H^2}} = \frac{1}{2 \cdot 0.5} = 1 \text{ s}.$$

However, during this time (Δ = 1 s) the magnetization of the sample disappears almost completely (due to relaxation) and, therefore, the sensitivity of the 2D J-HMBC experiment becomes very low.

In the 2D selective *J* spectrum[66, 67] (Fig. 17), the long-range SSCC $^{n}J_{C,H}$ and chemical shifts of the ^{13}C nuclei are plotted alongside different dimensions of the 2D spectrum.



To obtain the 2D selective *J* spectrum, the signal of one of the protons of the system is subjected to preliminary excitation. As a result, the correlation peaks corresponding to the ^{13}C carbon atoms coupled by the long-range SSCC with the excited proton are split along the *J* axis (F1 dimension) into doublets with couplings equal to the SSCC (see Fig. 17). For the excitation of the proton signal, one should use highly selective pulses to avoid the perturbation of the resonance lines of the satellites caused by the direct SSCC $^{1}J_{C,H}$ (the $^{1}J_{C,H}$ values range from 125 to 220 Hz). The high selectivity of the pulse is achieved due to the long time of signal excitation (20–50 ms), which corresponds to a selectivity of 50–20 Hz,[66] and to the power decrease. Thus, only the long-range constants $^{n}J_{C,H}$ are modulated during the period t_1 of this experiment, and their values for oligo- and polysaccharides do not exceed 10 Hz. Hence, a small spectral window SW $\leqslant$ 20 Hz is usually used when measuring F1 (*J* dimension) in the 2D *J*

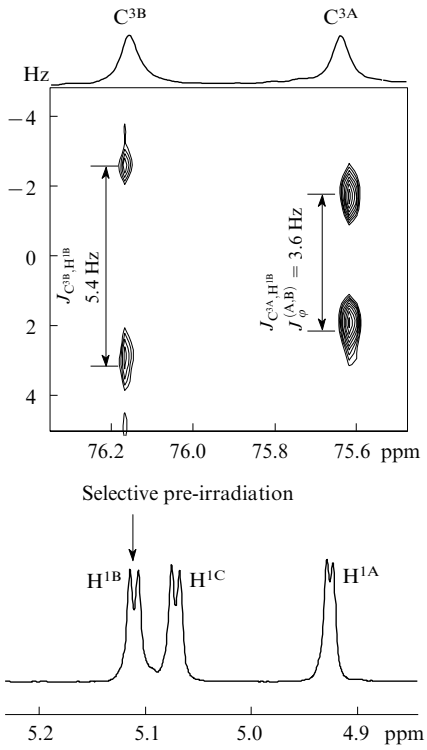


Figure 17. A fragment of the 2D selective *J* spectrum of trifucoside **6** (spectrometer 500 MHz, D_2O, 303 K)[75] containing the correlation peaks of the carbon atoms C^{3A} and C^{3B}.
These signals are split due to the spin–spin interactions with H^{1B} irradiated during the experiment.

experiment, which makes it possible to obtain a very good resolution (at a small number of points detected along the coordinate t_1) and to measure the values of the coupling constants with high accuracy. In the case of trifucoside **6**, the transglycosidic coupling constant $J_{\varphi}^{(A,B)}$ = 3.6 Hz was determined using the *J* spectrum (see Fig. 17).[75, 76]

Recently, it has become possible to use non-rectangular excitation pulses[77–80] that enhance the selectivity. The Gaussian pulse[77, 78] (Fig. 18) is one of the most frequently used selective pulses. In the frequency representation, this

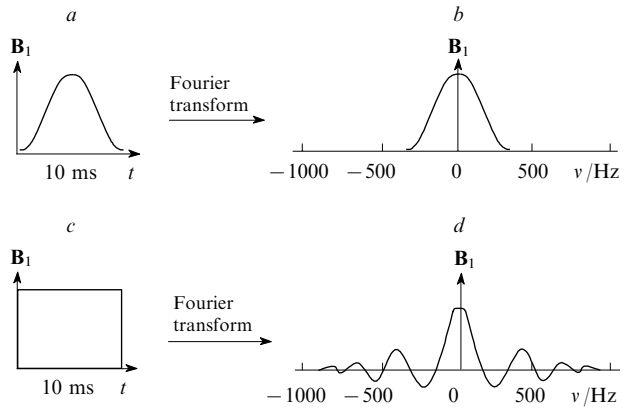


Figure 18. Selective pulses of the Gaussian (*a*) and rectangular (*c*) shapes and their Fourier images (frequency representations) (*b* and *d*, respectively).

pulse, unlike the rectangular one (see Fig. 18), has no undesirable wiggles at the edges of the excitation range and, hence, does not perturb the signals of the protons neighbouring to the excited proton.

The nuclear Overhauser effect that emerges on the ^{13}C nuclei upon the pre-irradiation of protons is usually employed to enhance the sensitivity of the 2D *J* experiment. For this purpose, in the beginning of the experiment, all protons are subjected to the excitation with the weak electromagnetic field during the relaxation delay t_{rel} (about 1–5 s). The sensitivity of the 2D *J* experiment can also be increased due to the transfer of polarization from protons to the ^{13}C carbon atoms. In this case, the sequences DEPT,[81] INEPT[82] or PENDANT are incorporated into the beginning of the sequence of the *J* experiment.[67]

An advantage of the 2D selective *J* experiment is the small number of correlation peaks in the spectrum, which decreases the probability of their overlap. Only one splitting caused by the particular SSCC corresponds to each carbon atom bound by the long-range coupling constant $^{n}J_{C,H}$ to the excited proton; the ^{13}C chemical shifts and SSCC are plotted on different axes (F2 and F1, respectively). In some cases, this helps to determine the $^{n}J_{C,H}$ values in this experiment, while other experiments are inefficient. For instance, the transglycosidic coupling constant $J_{\varphi}^{(B,C)} = J_{C^{3B},H^{1C}} = 3.8$ Hz (Fig. 19) was determined from the 2D J-HMBC spectrum of trifucoside **6**. However, it was impossible to determine the $J_{\varphi}^{(A,B)} = J_{C^{3A},H^{1B}}$ value because of the overlap of the correlation peaks C^{3A}/H^{1B} and C^{3B}/H^{1B}. This constant was determined from the 2D selective *J* spectrum (see Fig. 17): $J_{\varphi}^{(A,B)} = 3.6$ Hz.

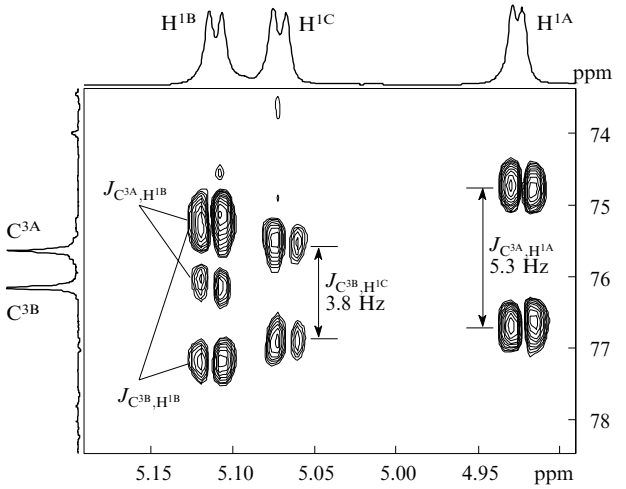


Figure 19. A fragment of the 2D J-HMBC spectrum of trifucoside **6** (500 MHz spectrometer, D_2O, 303 K)[75] reflecting the interactions of C^{3A} and C^{3B} with the anomeric protons H^{1A}, H^{1B} and H^{1C}.

A disadvantage of the selective *J* experiment is that the corresponding spectrum contains information about the SSCC of the carbon atoms with only one irradiated proton. To determine the SSCC values with another proton, it is necessary to repeat the experiment with the selective pulse at the resonance frequency of the corresponding proton. It should be mentioned that the sensitivity of this experiment is somewhat lower compared to the GATED, J-HMBC and HSQMBC experiments.

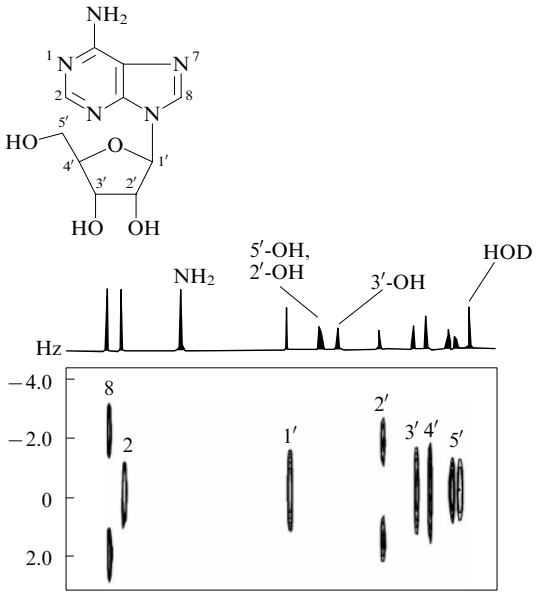


Figure 20. The inverted 2D selective *J* spectrum of adenosine (400 MHz spectrometer, DMSO-d_6, 303 K).[67]
The correlations corresponding to $H^{2'}$ and H^{8} are split into doublets due to the spin–spin interactions of the atoms $C^{2'}$ and C^{8} with the selectively inverted proton $H^{1'}$.

The pulse sequence of the inverted 2D selective *J* experiment was described[67] (Fig. 20) in which the ^1H NMR spectrum of the compound under study is plotted along side the F2 axis. The correlation peaks corresponding to the protons that are directly bound to the ^{13}C atoms that have long-range SSCC with the selectively irradiated proton are split into doublets with the magnitude of this SSCC.

Yet another class of NMR experiments providing information about the long-range heteronuclear SSCC is presented by experiments of the E.COSY type[45,46] (X-filtred 2D NOESY, TOCSY or RELAY COSY[68–70]). In the corresponding 2D spectra, the cross-peaks corresponding to proton couplings are split due to the heteronuclear SSCC. In this case, the type of splitting is analogous to the splitting of correlations in the E.COSY spectra (Fig. 21).

For example, in the X-filtred 2D NOESY experiment[68,69] the cross-peaks are split alongside one axis due

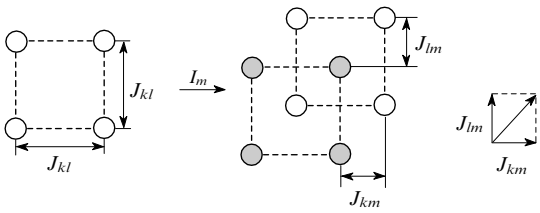


Figure 21. The shape of cross-peaks in the E.COSY spectra.
The cross-peak corresponding to the interaction of the nuclear spins I_k and I_l in the three-spin system $I_kI_lI_m$ is shown. The constant J_{kl} causes the cross-peak splitting into four components arranged at vertices of the square. This square is replicated due to the SSCC J_{km} and J_{lm} between the active spins *k* and *l* and the passive spin *m*. To determine the SSCC values J_{km} and J_{lm} from the multiplicity of the cross-peak, it is necessary that at least one of these SSCC is large to provide the resolution of the components of the cross-peak relative to each other.

to the direct heteronuclear coupling constant $^1J_{X,H}$ with one of the interacting protons, whereas the splitting alongside the second coupling constant is due to the long-range constant $^nJ_{X,H}$ with another interacting proton. As a rule, direct heteronuclear coupling constants $^1J_{X,H}$ are large, which favours the resolution of the multiplet components and thus makes it possible to determine small long-range coupling constants $^nJ_{X,H}$. The direct ($^1J_{X,H}$) and long-range ($^nJ_{X,H}$) heteronuclear coupling constants in the cross-peaks of the proton correlation spectra are plotted alongside different axes (F1 and F2), because the magnetization caused by the NOE between two protons during the period t_1 evolves at the frequency of one proton, whereas during the period t_2 its evolution occurs at the frequency of the other proton.

Note that the determination of the heteronuclear SSCC $^nJ_{C,H}$ of oligo- and polysaccharides using the E.COSY experiments requires the sample to be enriched in the ^{13}C carbon magnetic isotope at the X nucleus by 100%. Otherwise, the cross peaks corresponding to the ^{13}C and ^{12}C carbon isotope nuclei will overlap, which makes impossible the determination of the long-range heteronuclear coupling constants $^nJ_{C,H}$. However, in studies of oligo- and polysaccharides, one seldom deals with samples enriched in the ^{13}C isotope by 100%. Therefore, the use of X-filtred 2D NOESY, TOCSY and RELAY COSY experiments, for the study of such compounds, including their conformational analysis, is practically uncommon.

Remind that the $^1H-^1H$ E.COSY homonuclear experiment,[43,45,46] its modification PE.COSY[43,47] and the $^1H-^{13}C$ XLOC heteronuclear experiment[50–52] in which the shape of the cross peaks is the same as that in the E.COSY spectra, can also be used for the determination of the coupling constants $J_{H,H}$.

IV. Modern methods for registration of the nuclear Overhauser effect and specific aspects of its use in conformational analysis of oligo- and polysaccharides

The phenomenon of the nuclear Overhauser effect is the change in the NMR signal intensity of a nucleus upon saturation of the resonance of another nucleus interacting with the former through the dipole–dipole mechanism.[83] The NOE value (f_k^d) is defined as the ratio of the change in the signal intensity d under the conditions of saturation of the nucleus k to its intensity in the absence of saturation [Eqn (9a)].

$$f_k^d = \frac{I_d - I_d^0}{I_d^0}, \tag{9a}$$

where I_d^0 is the signal intensity of the nucleus d in the NMR spectrum in the absence of resonance saturation of the nucleus k, I_d is the signal intensity d upon resonance saturation of the nucleus k. The signal intensities (I) in the NMR spectra are directly proportional to the longitudinal nuclear magnetization values (S) and, hence, Eqn (9a) can be written as Eqn (9b):

$$f_k^d = \frac{S_d - S_d^0}{S_d^0}. \tag{9b}$$

The nuclear Overhauser effect is a consequence of the tendency of a system of interacting nuclei to reach the thermal equilibrium state upon the change in the occupanices of the spin states of the nucleus k. This process is accompanied by the excess energy redistribution to other nuclei of the system bound by the dipole–dipole interaction, which results in a change in the signal intensities of the non-irradiated nuclei.

Thus, the NOE, unlike SSCC, can be used for studies of the mutual spatial arrangement of nuclei separated by many bonds. In the case of oligo- and polysaccharides, the NOE values can be used for both the establishment of the configuration of monosaccharide residues (from the NOE values between the protons of the same ring, Fig. 22) and the study of solution conformations of these molecules. In

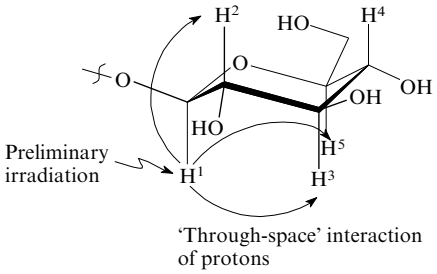


Figure 22. Interactions of protons in the β-L-glucopyranose residue leading to the NOE upon the irradiation of the proton H^1.

the latter case, the NOE values between the protons separated by the glycosidic bonds are the most significant (Fig. 23). The NOE values emerging on protons of the glycosylated residue upon pre-irradiation of the anomeric proton (H^1) of the glycosylating residue (see Fig. 23) are most often studied in conformational analysis of oligo- and polysaccharides. This figure shows that the proton–proton interactions observed help to draw complete conclusions about the conformations of the disaccharide fragment of a substance under study.

The pulse sequence of the experiment for the detection

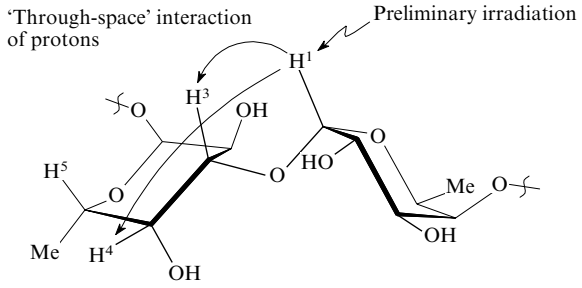


Figure 23. An example of interaction of protons from different residues of a disaccharide fragment leading to the NOE upon the irradiation of the proton H^1 of the 'glycosylating' residue.

of the NOE between protons differs from that of a standard ^1H NMR experiment in the prolonged low-power radiofrequency radiation (CW) with the frequency corresponding to the resonance of the proton k (Fig. 24).[32] The NOE develops in the system within this time period (τ_s), changing the intensity of the detected signals.

Difference NOE spectra are usually considered in practice to minimize the artifacts appearing due to radiofrequency radiation (CW). For this purpose, the spectrum in

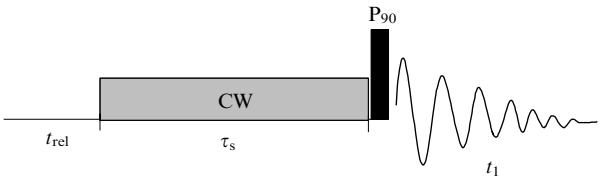


Figure 24. Pulse sequence in the experiment for recording the proton NOE (see text).[84]

which the irradiation frequency (CW) corresponds to the frequency of the saturated signal k is recorded first. Then the spectrum in which the radiation frequency falls into the spectral region free of signals is detected. The subtraction of these two spectra gives the difference NOE spectrum.

The NOE value observed for signals of other protons of the system change with the irradiation time (τ_s) of the proton k (see Fig. 24). The general view of the dependence of the NOE value for the proton d (f_k^d) on the irradiation time of the proton k is shown in Fig. 25. The plot shows that at first the NOE is gradually enhanced with the elongation of the irradiation time of the nucleus; however, at the longer irradiation times the NOE value reaches a plateau, which corresponds to a new steady state achieved by the system.

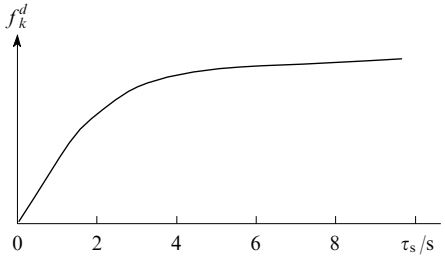


Figure 25. Dependence of the NOE value for the proton d (f_k^d) on the irradiation time of the proton k.

Experiments on the steady-state and transient NOE are distinguished depending on the duration of irradiation of the system.[84] In the former case, the difference in occupancies of transitions of the nucleus k is perturbed for such a long time that the system has time to achieve the new steady state. It is usually necessary that the irradiation time exceeds the longest relaxation time in the molecule by a factor of two to three (for protons in the carbohydrate derivatives this time is $\sim 7-9$ s).

Noggle and Schirmer obtained[83] the equation for the calculation of the proton–proton steady-state NOE values in molecules

$$f_k^d = \left\{ \left[\frac{6\tau_c}{1+(2\omega_0\tau_c)^2} - \tau_c \right] \Big/ \left[\frac{3\tau_c}{1(2\omega_0\tau_c)^2} + \tau_c + \frac{6\tau_c}{1+(2\omega_0\tau_c)^2} \right] \right\} \times$$
$$\times \left(\frac{r_{dk}^{-6}}{\sum\limits_{j\neq d} r_{dj}^{-6}} - \sum_{j\neq k,d} \frac{r_{dj}^{-6} f_k^j}{\sum\limits_{j\neq d} r_{dj}^{-6}} \right), \qquad (10)$$

where r_{dj} is the distance between the protons d and j, τ_c is the time of isotropic rotational correlation.

Thus, the steady-state NOE (f_k^d) depends on several factors, first of all, on the distance between the saturated proton k and the observed proton d (inversely proportional to r_{dk}^6), on the correlation time of the protons τ_c and on the Larmor frequency of the protons ω_0 (Fig. 26). It should be emphasized that Eqn (10) was obtained under assumption that the predominant contribution to the relaxation is made by the intramolecular dipole–dipole interaction of protons. If other mechanisms contribute substantially to the relaxation, the real NOE value will be lower than that calculated by Eqn (10).

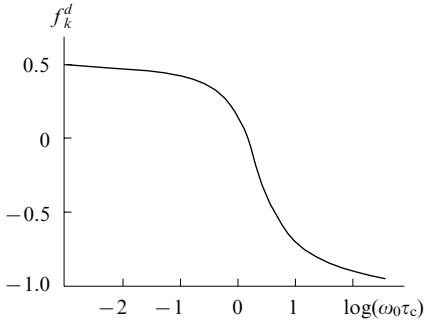


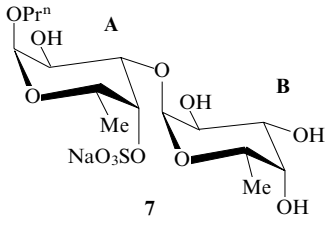
Figure 26. Dependence of the NOE value on the product $\omega_0\tau_c$.[83]

For small organic molecules, the correlation times lie in the interval $10^{-12} < \tau_c < 10^{-10}$ s; for example, for the monosaccharide residues $\tau_c \approx 10^{-11}$ s, and for disaccharides $\tau_c \approx 10^{-10}$ s. At an instrumental frequency of 500 MHz, the Larmor frequency of protons $\omega_0 \approx 10^9$ and, therefore, $\omega_0^2\tau_c^2 \ll 1$. In this case, the expression in braces of Eqn (10) is equal to 0.5 and, thus, Eqn (10) is simplified to

$$f_k^d = \frac{r_{dk}^{-6}}{2\sum\limits_{j\neq d} r_{dj}^{-6}} - \sum_{j\neq k,d} \frac{r_{dj}^{-6} f_k^j}{2\sum\limits_{j\neq d} r_{dj}^{-6}}. \qquad (11)$$

These systems are characterized by the positive NOE, *i.e.*, the signal resonance of the observed proton d increases upon the resonance saturation of the proton k. In the case of the system of two interacting protons, the value $f_k = 0.5$ is independent of the distance between the irradiated and observed protons. The value $f_k d = 0.5$ is the maximum positive NOE, which can be achieved in the system of interacting protons. The condition $\omega_0^2\tau_c^2 \ll 1$ is called the extreme narrowing limit and corresponds to the total disappearance of the dipole–dipole-induced line broadening in the NMR spectra.

We used the steady-state NOE values for the comparative conformational analysis of propyl 3-*O*-(α-L-fucopyranosyl)-α-L-fucopyranoside (**3**) and its C^4-sulfated derivative **7** (Fig. 27).[85]



For this purpose, selective saturation of the resonance of the H^1 proton of the glycosylating residue was carried out, which resulted in emerging of the NOE on signals of H^3, H^4 and H^5 of the glycosylating residue **A** (Figs 27 and 28,

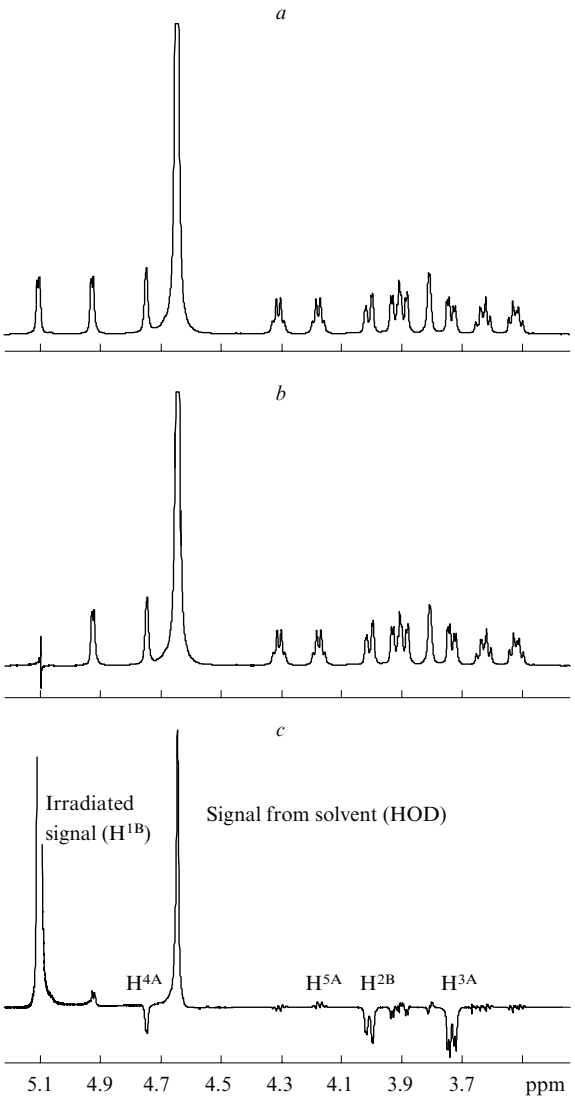
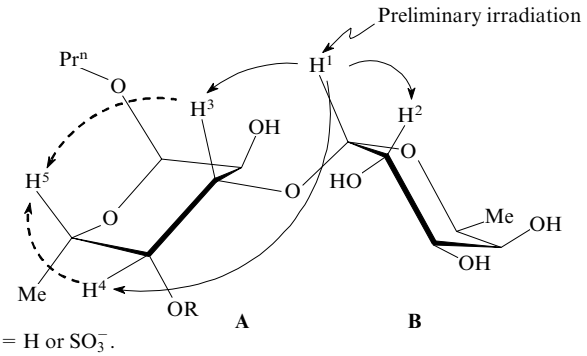


Figure 27. Determination of the steady-state NOE in difucoside **7**.[85] (*a*) ^{1}H NMR spectrum of difucoside **7** obtained by the pulse sequence of the NOE experiment (see Fig. 24); the signal-free spectral region was subjected to the radiofrequency irradiation (CW); (*b*) spectrum of the steady-state NOE of difucoside **7** obtained due to the saturation of the resonance of the proton H^{1B} for 7.2 s (500 MHz spectrometer, D_2O, 307 K); (*c*) difference NOE spectrum obtained by the subtraction of spectrum *b* from spectrum *a* (the intensity of spectrum *c* was amplified for clarity relative to spectra *a* and *b*). The main signals caused by the NOE are marked in the spectrum.

Table 5). It was found that the sulfation of the OH group at C^4 in the disaccharide decreased the NOE value for the H^4 from 88.8% to 41.5%. At the same time, the theoretical conformational analysis performed for these compounds[85] and based on the molecular mechanics calculations (force field MM3) showed two conformers (**I** and **II**) for the (1→3)-linked disaccharide fragments of these molecules (Fig. 29). The transition from disaccharide **3** to sulfated disaccharide **7** was accompanied by a decrease in the fraction of conformer **I**. The NOE values calculated by the molecular mechanics and Eqn (11) agreed well with the experimental values (see Table 5), indicating that the molecular modelling is reliable.



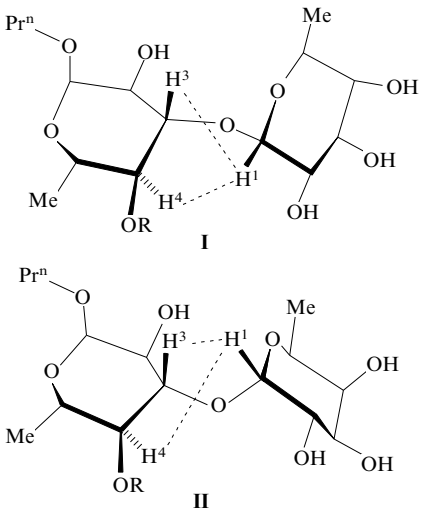
R = H or SO_3^-.

Figure 28. Principal NOE interactions in difucoside **3** and C^4-sulfated difucoside **7** appearing upon the saturation of the resonance of the proton H^1 of the glycosylating residue **B**.
Solid arrows mark the direct NOE interactions (positive), and dashed lines indicate the secondary NOE interactions (negative).

Table 5. Experimental (500 MHz spectrometer, D_2O) and calculated relative values of the steady-state NOE observed on protons of the glycosylated residue in difucoside **3** and C^4-sulfated difucoside **7** upon saturation for 7.2 s of the resonance of the proton H^1 of the glycosylating residue **B**.[85]

Compound	Proton	NOE (%)	
		experiment	calculation
Difucoside **3**	H^3	100	100
	H^4	88.8	85.0
	H^5	−12.9	−14.1
C^4-Sulfated difucoside **7**	H^3	100	100
	H^4	41.5	49.0
	H^5	−13.3	−11.9

It is of special note that the negative NOE values are observed for the H^5 of difucoside **3** and its C^4-sulfated derivative **7** (see Table 5), which is not characteristic of direct proton–proton NOE at the extreme narrowing limit ($\omega_0^2\tau_c^2 \ll 1$) and is due to spin diffusion.[53,84] The matter is



R = H or SO_3^-.

Figure 29. Characteristic conformers **I** and **II** of difucoside **3** and its C^4-sulfated derivative **7**.[85]

that along with direct proton pair interactions secondary effects can occur, that are due to the transmission of the perturbation induced in the molecule through the proton chain. For instance, in difucosides **3** and **7**, the presaturation of the resonance of the H^1 proton of the glycosylating residue (**B**) changes the difference in the level occupancies of H^3 and H^4 of the glycosylating residue (**A**) (see Fig. 28) resulting in the appearance of the positive NOE. These protons in turn affect H^5 (spin diffusion) inducing the NOE of an opposite sign on this proton. In this case, no direct NOE is observed for H^5, because the latter is remote from the irradiated proton H^1. In addition to the NOE signals in the spectrum (see Fig. 27 *c*), there are small false signals characterized by a distorted phase. These signals appear because the magnetic field of the spectrometer is unstable in time and the electromagnetic pulses are inaccurately reproduced, which results in the non-ideal subtraction of spectra *a* and *b*.

A situation where $\omega_0\tau_c \approx 1$ and no NOE is observed ($f_k^d = 0$) can appear for molecules of medium size. This means that the signal of the proton in question disappears completely in the NOE spectrum. Indeed, at $\omega_0\tau_c = 1.118$, the numerator in Eqn (10) is zero. At a frequency of the instrument of 500 MHz, the corresponding τ_c value is 3.5×10^{-10} s.

If $\omega_0^2\tau_c^2 \gg 1$ ($\tau_c > 3.5 \times 10^{-10}$ s satisfies this condition), the expression in braces in Eqn (1) becomes equal to -1 and the formula for the calculation of the NOE value takes the following form:

$$f_k^d = -\frac{r_{dk}^{-6}}{\sum\limits_{j\neq d} r_{dj}^{-6}} + \sum_{j\neq k,\,d} \frac{r_{dj}^{-6} f_k^j}{\sum\limits_{j\neq d} r_{dj}^{-6}}. \qquad (12)$$

Thus, the negative NOE values are observed in solutions with high viscosity or in solutions of large molecules (higher oligosaccharides, polysaccharides, *etc*.). For the system of two protons, under these conditions $f_k^d = -1$, which is a minimum possible value of the NOE.

The fact that the first term in Eqns (11) and (12) considerably exceeds the components of the second sum opens a way for the determination of the NOE values by the iteration method. For this purpose, the following parameters

$$\frac{r_{dk}^{-6}}{\sum\limits_{j\neq d} r_{dj}^{-6}},$$

are calculated from the distances between protons and substituted into the full equations of the NOE (10)–(12), and this gives the refined values.

The experiment on the steady-state NOE is highly sensitive. A serious drawback of this procedure is that it requires the preliminary selective irradiation of one of the resonance lines in the ^{1}H NMR spectrum. Thus, the procedure of measuring the steady-state NOE can successfully be used for molecules with well resolved ^{1}H NMR signals.

In the case of experiments on the transient NOE, the irradiation times used are considerably shorter than those necessary for the establishment of a new steady state in the system.[84] The pulse sequence somewhat different from that presented in Fig. 24 is usually applied. This is the so-called 1D NOESY experiment (Fig. 30).

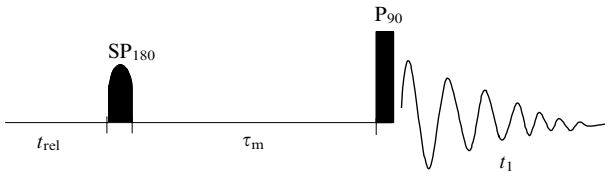


Figure 30. Pulse sequence in a 1D NOESY experiment (for clarifications, see text).

In the first stage of experiments on the transient NOE (see Fig. 30), as well as in experiments on measuring the steady-state NOE, the difference in site occupanices of the energy levels of the irradiated nucleus k is perturbed. However, in transient NOE experiments the magnetization of the nucleus k is inverted (the magnetization vector is directed along the axis $-z$), unlike the steady-state NOE method, where the occupanices of the energy levels of the nucleus k (saturation of transitions of the nucleus k) are equalized. The inversion of the signal of the proton k is achieved by the selective 180° pulse (SP_{180}) at the frequency of this proton (ν_k). After the action of the selective pulse during the time τ_m, which is called the mixing time, the perturbation introduced into the site occupanices of energy levels of the nucleus k is redistributed to other protons of the system (the appearance of the NOE). Then the non-selective 90° pulse (P_{90}) transmits the magnetization vectors of protons to the plane xy where they are detected as the FID by the receiver coil of the NMR spectrometer.[32] Note that the selective non-rectangular pulse (for example, the Gaussian pulse, see Fig. 18) is used in 1D NOESY experiments. This allows one to affect the signals neighbouring the irradiated one to a lesser extent than in the case of the steady-state NOE experiments and thus to measure the NOE with a higher accuracy.

The general view of the dependence of the transient NOE for the proton d on the mixing time τ_m is shown in Fig. 31. It can be seen that at short times τ_m the dependence is linear as that in Fig. 25. The initial NOE increase for the nucleus d is proportional to the cross-relaxation constant (R_{kd}) between the irradiated (k) and observed (d) protons even in the multispin system

$$\frac{dS_d}{dt} \propto R_{kd}. \qquad (13)$$

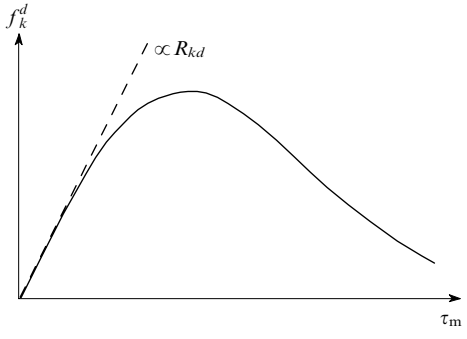


Figure 31. Dependence of the non-steady-state NOE for the proton d (f_k^d) upon irradiation of the proton k on the mixing time τ_m.[53]

The cross-relaxation rate constant is given by the expression

$$R_{kd} = \frac{1}{10}\left(\frac{\mu_0}{4\pi}\right)^2 \gamma^4 h^2 \left(\frac{6\tau_c}{1+(2\omega_0\tau_c)^2} - \tau_c\right)\frac{1}{r_{kd}^6}, \qquad (14)$$

where μ_0 is the magnetic constant of vacuum, γ is the gyromagnetic ratio of the proton, and h is Planck's constant.

Expression (13) is the so-called condition of initial approximation of the rate of growth of the transient NOE.[53] At short times τ_m, a pair of nuclei behaves in such a way as if they were an isolated system with the NOE value between them proportional to τ_m. At longer mixing times, the relaxation rate of the nucleus d becomes comparable with the cross-relaxation rate, which induces the deviation of the NOE function from a linear law and its decrease to zero at $\tau_m \gg T_1$ (T_1 is the longitudinal relaxation time for the nucleus d). Thus, the initial approximation condition can be applied only to the mixing times $\tau_m \ll T_1$.

Since the cross-relaxation rate constant R_{kd} between the observed (d) and irradiated (k) protons is inversely proportional to the sixth power of the distance between these atoms (r_{kd}^{-6}) [Eqn (14)], the following equation can easily be obtained from relation (13)

$$f_k^d = c r_{kd}^{-6} \tau_m, \qquad (15)$$

where c is the constant including the fundamental constants and the correlation time of the molecule (τ_c).[53] Equation (15) can directly be used for the determination of the interproton distances r_{kd} from the known NOEs. The correlation time can be determined from the data on the relaxation times T_1 of the ^{13}C nuclei.[86]

In practice, the reproducible measurement of the NOE values depends on several experimental conditions: the concentration and nature of the sample, the presence of paramagnetic impurities, the degree of saturation of irradiated signal transitions and specific properties of the instrument. However, the ratio of two NOEs within one molecule, which is refferred to as the relative NOE, is less sensitive to all these factors and inversely proportional to the sixth power of the ratio of the corresponding interproton distances.

$$\frac{f_k^d}{f_n^m} = \left(\frac{r_{kd}}{r_{nm}}\right)^{-6}. \qquad (16)$$

It is Eqn (16) that is used in practice for the determination of the spatial structure of molecules from experimental values of the transient NOE.

The observation of the transient NOE from the NOESY experiment can be carried out in both the one-dimensional (1D) and two-dimensional (2D) variants.[53,84] The 2D NOESY[87,88] spectrum contains information about all interproton NOEs of the molecule (Fig. 32). The 2D NOESY spectrum can theoretically be considered as a set of 1D spectra in each of which one proton of the system is selectively irradiated. To obtain the 2D NOESY spectrum, it is unnecessary to perform selective proton irradiation, which is usually impeded by signal overlapping in the 1D ^1H NMR spectrum.

Figure 32 *b* presents the 2D NOESY spectrum of *O*-antigenic polysaccharide of *Acinetobacter baumannii* O-7 (Ref. 89) containing six monosaccharide residues in the

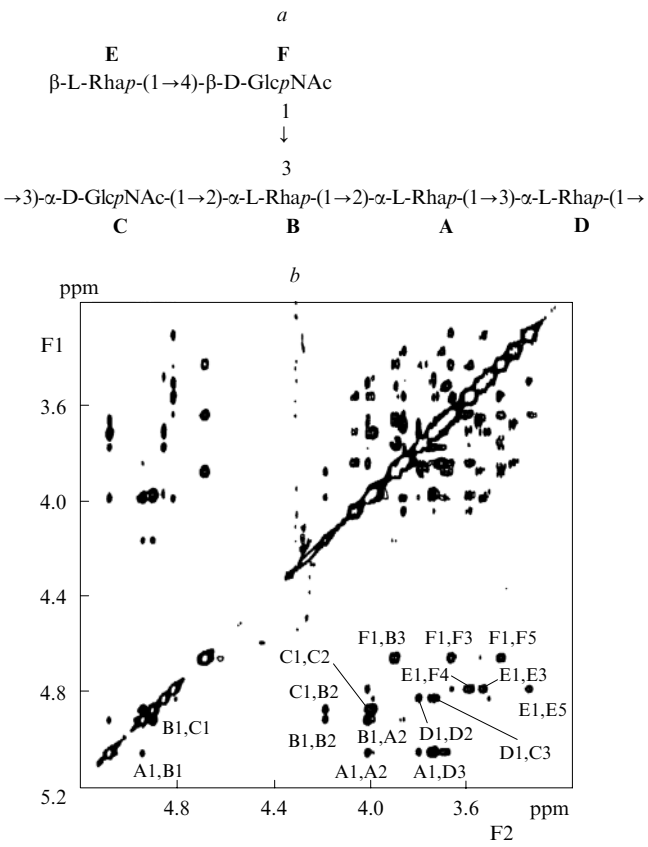
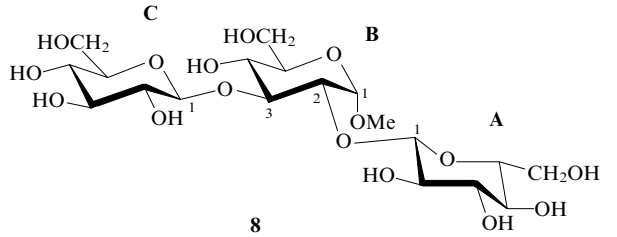


Figure 32. Primary structure (*a*) and the 2D NOESY spectrum (*b*) of *O*-antigenic polysaccharide of *Acinetobacter baumannii* O-7.[89] Non-diagonal peaks appear in the spectrum due to the NOE between the spatially close protons.

repeating unit (see Fig. 32 *a*): four of them (**A**–**D**) form the main polysaccharide chain and two residues are in the side group.

In the conformational analysis of polysaccharides and especially oligosaccharides, one should take into account the fact that these compounds are conformationally flexible and, as a rule, there is no just a single conformation that exactly corresponds to the experimentally detected NOE and SSCC values in the spectra. Therefore, in the simulation of carbohydrate molecules it is necessary to take into account the whole set of conformers or to average the results of the molecular dynamics calculation. For example, the molecular dynamics calculations of triglucoside **8** showed[90] a possibility for this compound to have several preferential conformers corresponding to the energy minima.



8

The averaged interproton distances found from the calculations coincided well with those obtained from the experimental NOEs (Table 6). At the same time, the SSCC

Table 6. Interproton distances calculated theoretically and from the experimental NOEs for 2,3-branched triglucoside **8**.[90]

Protons	Distances /Å	
	calculated from molecular dynamics data	calculated from experimental NOE values
$H^{1B}\cdots H^{2B}$	2.42	2.42
$H^{2B}\cdots H^{1A}$	2.28	2.25
$H^{3B}\cdots H^{1C}$	2.29	2.26
$H^{1B}\cdots H^{1A}$	3.01	3.16

Table 7. Calculated and experimental coupling constants $^3J_{C,H}$ for 2,3-branched triglucoside **8**.[90]

Interacting atoms	$^3J_{C,H}$ /Hz	
	calculation	experiment
H^{1A}/C^{2B}	3.9	3.8
H^{2B}/C^{1A}	3.7	4.5
H^{1C}/C^{3B}	3.6	3.9
H^{3B}/C^{1C}	6.0	4.9

values coincided worse (Table 7), although the tendencies for changing the constant values were reproduced by the calculations. This shows that it is useful to combine different procedures (for instance, NOE and SSCC measurement) in investigations of oligo- and polysaccharide conformations.

In conclusion, let us consider specific features of NOE observation of compounds for which $\omega_0\tau_c \approx 1$. The molecular weight of such compounds is usually 1000–2000 (depending on the solution viscosity and the resonance frequency of the NMR spectrometer used). For these molecules, the observed NOE values are close to zero and do not allow one to suggest conformations. This problem was solved by the introduction of ROESY experiments[91] into NMR spectroscopy where the nuclear Overhauser effect develops not in the powerful stationary magnetic field of the spectrometer ($\mathbf{B}_0$), but in the magnetic field $\mathbf{B}_1$ created by the transmitter of the NMR spectrometer. In this case, the NOE dynamics changes: $\gamma\mathbf{B}_1 \ll \gamma\mathbf{B}_0$ and, correspondingly, $\omega_1 \ll \omega_0$. As a result, the condition $\omega_1^2\tau_c^2 \ll 1$ is fulfilled for all real values τ_c and, therefore, all molecules behave in such a way as if they were at the extreme narrowing limit. The effects of the field $\mathbf{B}_0$ can be eliminated by the development of NOE in the plane xy perpendicular to the field direction $\mathbf{B}_0$. The pulse sequence of the 1D ROESY experiment is shown in Fig. 33.

In the first stage of the 1D ROESY experiment, as in the 1D NOESY experiment, the magnetization of proton k is inverted (the magnetization vector is directed along the axis $-z$) by the action of the selective pulse SP_{180}. The subsequent non-selective 90° pulse P_{90} transforms the magnetizations of all protons into the plane xy, where they are retained along the axis y by the low-intensity field $\mathbf{B_1}$ of the transmitter (spin-lock pulse) during the time τ_m. The situation during the action of the spin-lock pulse resembles that during the mixing time τ_m in the nonequilibrium 1D NOESY experiment, except for powers of the magnetic fields ($\mathbf{B}_0 \gg \mathbf{B}_1$) in which the NOE develop.

The ROESY experiments (as well as NOESY) are mainly carried out in the two-dimensional version. However, the measurement of the experimental NOE values in the ROESY spectra is associated with additional difficulties because of the appearance of correlations (TOCSY peaks) between the spin–spin coupled protons.[92] This is due to the fact that the spin-lock pulse[91] used in the ROESY experiment for the NOE development is similar to the pulse for the development of the Hartmann–Hahn[93] effect in the TOCSY experiment.

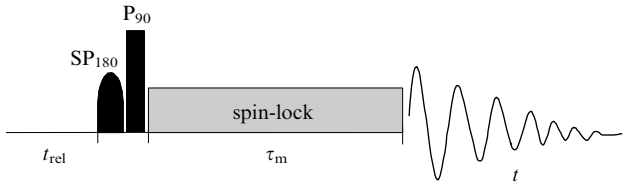
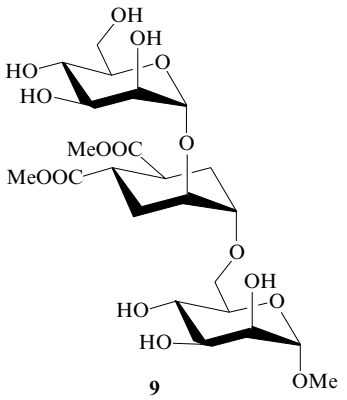


Figure 33. Pulse sequence in a 1D ROESY experiment (see text).

The conformational analysis of pseudo-trisaccharide **9**, which is a structural relative of (1→2),(1→6)-linked mannotrioside, was carried out[94] on the basis of the ROESY spectrum.

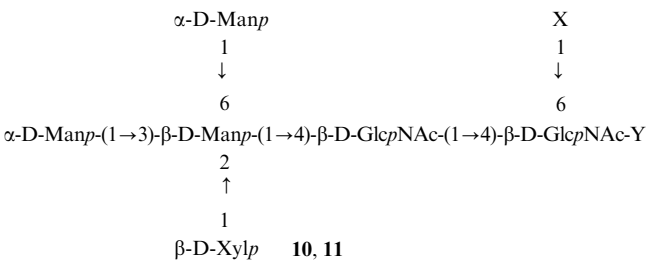


9

In the ^{1}H NMR spectra of compound **9**, which were recorded with spectrometers equipped with weak and medium magnetic fields, the signals of many protons overlapped and, hence, the instrument with a strong magnetic field (800 MHz) was used to study this molecule. In this case, in the ^{1}H NMR spectrum the signals of some protons still overlapped, but the number of such signals was much less. The spatial structure of pseudo-trisaccharide **9** was determined on the basis of the experimental NOE values. To determine the latter, the 2D ROESY experiment was used, because the condition $\omega_0\tau_c \approx 1$ was fulfilled for this compound on a spectrometer with a resonance proton frequency of 800 MHz, and the NOESY experiment was poorly informative. The ROESY spectrum made it possible to determine the preferential conformations of pseudo-trisaccharide **9** and to compare them with the conformations of the corresponding (1→2),(1→6)-linked mannotrioside.

At the same time, it was shown[95] that the NOESY experiment is preferable for the determination of the spatial structures of hexa- (**10**) and heptasaccharides (**11**), which are the fragments of the *N*-glycan of α_D-hemocyanine of snail *Helix pomatia*. The NOE values observed in the NOESY spectra (500 MHz spectrometer, D_2O, 282 K) were negative ($\omega_0^2\tau_c^2 > 1$). The ROESY spectra also gave information about the spatial structures of oligosaccharides

10 and **11**; however, the data obtained were less accurate because of many TOCSY peaks that were present in the spectra and overlapped with the ROESY peaks. The conformational analysis of hexa- and heptasaccharides **10** and **11** based on the experimental NOE values and molecular dynamics calculations made it possible to determine that the disaccharide fragments α-D-Man*p*-(1→6)-β-D-Man*p*, α-L-Fuc*p*-(1→6)-β-D-Glc*p*NAc and α-D-Man*p*-(1→3)-β-D-Man*p* were characterized by the presence of several conformational minima, whereas one preferential conformation existed for the fragment β-D-Xyl*p*-(1→2)-β-D-Man*p*-(1→4)-β-D-Glc*p*NAc-(1→4)-β-D-Glc*p*NAc.[95]



10, **11**

X = H (**10**), α-L-Fuc*p* (**11**); Y = (1→OMe).

V. Conclusion

Concluding the consideration of the methods for recording SSCC and NOE by NMR spectroscopy and the application of these spectral parameters to the conformational analysis of oligo- and polysaccharides in solution, it can be noted that experiments on determination of heteronuclear SSCC $J_{C,H}$ are less sensitive than of the proton–proton NOE. This is mainly due to the low natural abundance of the ^{13}C carbon isotope (1.1%) in organic compounds and the lower magnetization of the ^{13}C nuclei compared to the ^{1}H protons (the interrelation of the gyromagnetic ratios of these nuclei γ_H/γ_C is 3.971). Therefore, the exact determination of experimental values of the coupling constants $J_{C,H}$ is often a very difficult problem that sometimes cannot be solved experimentally. At the same time, an advantage of experiments on the determination of heteronuclear coupling constants $J_{C,H}$, especially in the two-dimensional version, over the NOE experiments is their higher resolution. When the SSCC $J_{C,H}$ are recorded by 2D NMR spectroscopy, one of dimensions of the spectrum usually corresponds to the chemical shifts of the ^{13}C nuclei, which in oligo- and polysaccharides vary in a much broader range (0–110 ppm) than the chemical shifts in ^{1}H NMR spectra (0–6 ppm). The problem of spectra resolution becomes especially topical in the case of higher oligosaccharides and polysaccharides containing tens and even hundreds of non-equivalent nuclei.

It should be emphasized that the SSCC and NOE values reflect changes in the molecular geometry in different manners. The vicinal SSCC are proportional to the squared cosine of the corresponding dihedral angle ($\cos^2\theta$), whereas the NOE values are inversely proportional to the sixth power of the distance between the interacting atoms (r^{-6}). Therefore, the structural conclusions obtained on the basis of determination of SSCC and NOE can substantially supplement each other when used in the conformational analysis of carbohydrates. It should be taken into account that the experimental NOE and SSCC values are averaged over all accessible conformations of carbohydrates in solution. The same averaged values can be obtained by theoretical conformational analysis based on the molecular and quantum mechanics method. That is why the cooperative analysis of the experimental results considered in the present review and the theoretical studies makes it possible to obtain the most comprehensive conclusions about the spatial structures of oligo- and polysaccharides in solution.

The authors are grateful to D.Sc. (Chemistry) V I Pol'shakov, Ph.D. (Chemistry) Yu A Strelenko and D.Sc. (Chemistry) A I Usov for critical consideration of the review and helpful remarks.

This work was financially supported by the Russian Foundation for Basic Research (Project No. 08-03-00 884-a) and the Programme of Grants of the President of the Russian Federation for Support of Young Scientists (Grants MK-5970.2008.3 and MK-5879.2008.3).

References

1. W T J Morgan, W M Watkins *Br. Med. Bull.* **25** 30 (1969)
2. W M Watkins, in *Advances in Human Genetics* Vol. 10 (Eds H Harris, K Hirschhorn) (New York: Plenum, 1980) p. 1
3. J V Höltje, U Schwarz, in *Molecular Cytology of Escherichia Coli*. (London: Academic Press, 1985) p. 77
4. E T Rietschel, H Brade *Sci. Am.* **267** 54 (1992)
5. L Kjellén, U Lindahl *Annu. Rev. Biochem.* **60** 443 (1991)
6. M Yanagishita *Experientia* **49** 366 (1993)
7. M L Phillips, E Nudelman, F C A Gaeta, M Perez, A K Singhal, S I Hakomori, J C Paulson *Science* **250** 1130 (1990)
8. G Walz, A Arufto, W Kalanus, M Bevilacqua, B Seed *Science* **250** 1132 (1990)
9. J B Lowe, L M Stoolman, R P Nair, R D Larson, T L Berhend, R M Marks *Cell* **63** 475 (1990)
10. A Chandrasekaran, A Srinivasan, R Raman, K Viswanathan, S Raguram, T M Tumpey, V Sasisekharan, R Sasisekharan *Nat. Biotechnol.* **26** 107 (2008)
11. K T Welch, T A Turner, C E Preast *Bioorg. Med. Chem. Lett.* **18** 6573 (2008)
12. H Xin, S Dziadek, D R Bundle, J E Cutler *Proc. Natl. Acad. Sci. USA* **105** 13526 (2008)
13. J Tejler, F Skogman, H Leffler, U J Nilsson *Carbohydr. Res.* **342** 1869 (2007)
14. M L Gening, Y E Tsvetkov, G B Pier, N E Nifantiev *Carbohydr. Res.* **342** 567 (2007)
15. R Schwartz-Albiez, Y Adams, C-W von der Leith, P Mischnick, K T Andrews, M Kirschfink *Glycoconjugate J.* **24** 57 (2007)
16. D Schwizer, H Gäthje, S Kelm, M Porro, O Schwardt, B Ernst *Bioorg. Med. Chem.* **14** 4944 (2006)
17. K Aplander, J Tejler, J Toftered, S Carlsson, B Kahl-Knutsson, A Sundin, H Leffler, U J Nilsson *Carbohydr. Res.* **341** 1363 (2006)
18. A Imberty, H Lortat-Jacob, S Pérez *Carbohydr. Res.* **342** 430 (2007)
19. A G Gerbst, A A Grachev, A S Shashkov, N E Nifantiev *Bioorg. Khim.* **33** 28 (2007) [a]
20. G M Lipkind, Doctoral Thesis in Chemical Sciences, Institute of Organic Chemistry, Academy of Sciences of the USSR, Moscow, 1991
21. P Finch *Carbohydrates. Structures, Syntheses and Dynamics* (Berlin: Springer, 1999
22. N Cyr, A S Perlin *Can. J. Chem.* **57** 2504 (1979)
23. S J Angyal *Carbohydr. Res.* **77** 37 (1979)
24. R U Lemieux, K Bock, L T J Delbaere, S Koto, V S Rao *Can. J. Chem.* **58** 631 (1980)
25. J A Schwarcz, A S Perlin *Can. J. Chem.* **50** 3667 (1972)
26. C Altona, C A G Haasnoot *Org. Magn. Reson.* **13** 417 (1980)

27. A S Shashkov, Z Pakulski, B Grzeszczyk, A Zamojski *Carbohydr. Res.* **330** 289 (2001)
28. B Mulloy, T A Frenkiel, D B Davies *Carbohydr. Res.* **184** 39 (1988)
29. I Tvaroška, M Hricovíni, E Peráková *Carbohydr. Res.* **189** 359 (1989)
30. F Cloran, I Carmichael, A S Serianni *J. Am. Chem. Soc.* **121** 9843 (1999)
31. F Heatley, L Akhter, R T Brown *J. Chem. Soc., Perkin Trans. 1* 919 (1980)
32. N M Sergeev *Spektroskopiya YaMR* (Spectroscopy of NMR) (Moscow: Moscow State University, 1981)
33. A A Shahkhatuni, A G Shahkhatuni *Usp. Khim.* **71** 1132 (2002) [*Russ. Chem. Rev.* **71** 1005 (2002)]
34. A S Shashkov, G M Lipkind, Y A Knirel, N K Kochetkov *Magn. Reson. Chem.* **26** 735 (1988)
35. D M Grant, B V Cheney *J. Am. Chem. Soc.* **89** 5315 (1967)
36. M Karplus *J. Chem. Phys.* **30** 11 (1959)
37. M Karplus *J. Am. Chem. Soc.* **85** 2870 (1963)
38. M J Minch *Concep. Magn. Reson., Part A* **6** 41 (1994)
39. C A G Haasnoot, F A A M de Leeuw, C Altona *Tetrahedron* **36** 2783 (1980)
40. A A Grachev, A G Gerbst, M L Gening, D V Titov, Yu E Tsvetkov, A S Shashkov, N E Nifantiev, in *The VIth International Congress of Young Chemists 'YoungChem 2008', Cracow, 2008* p. 110
41. D Marion, K Wüthrich *Biochem. Biophys. Res. Commun.* **113** 967 (1983)
42. F Delaglio, Z Wu, A Bax *J. Magn. Reson.* **149** 276 (2001)
43. J Cavanagh, W J Fairbrother, A G Palmer III, N J Skelton *Protein NMR Spectroscopy: Principles and Practice* (2nd Ed.) (New York: Academic Press, 2007)
44. M Rance, O W Sørensen, G Bodenhausen, G Wagner, R R Ernst, K Wüthrich *Biochem. Biophys. Res. Commun.* **117** 479 (1983)
45. C Griesinger, O W Sürensen, R R Ernst *J. Am. Chem. Soc.* **107** 6394 (1985)
46. C Griesinger, O W Sørensen, R R Ernst *J. Chem. Phys.* **85** 6837 (1986)
47. L Mueller *J. Magn. Reson.* **72** 191 (1987)
48. D Yang, X Xu, C Ye *Magn. Reson. Chem.* **30** 711 (1992)
49. S Simova *Magn. Reson. Chem.* **36** 505 (1998)
50. M D Sørensen, S M Kristensen, J J Led, O W Sørensen *J. Magn. Reson., Ser. A* **103** 364 (1993)
51. A Meissner, O W Sørensen *Magn. Reson. Chem.* **39** 49 (2001)
52. J Zhang, A Spring, M W Germann *J. Am. Chem. Soc.* **131** 5380 (2009)
53. T D W Claridge *High Resolution NMR Techniques in Organic Chemistry* (Oxford: Pergamon Press, 1999)
54. A A Karelin, Y E Tsvetkov, L Paulovičová, S Bystrickỳ, E Paulovičová, N E Nifantiev *Carbohydr. Res.* **344** 29 (2009)
55. R E Hurd *J. Magn. Reson.* **87** 422 (1990)
56. T Parella *Magn. Reson. Chem.* **36** 467 (1998)
57. P E Hansen *Prog. Nucl. Magn. Reson. Spectrosc.* **14** 175 (1981)
58. R Aydin, H Günther *Magn. Reson. Chem.* **28** 448 (1990)
59. R Stenutz, I Carmichael, G Widmalm, A S Serianni *J. Org. Chem.* **67** 949 (2002)
60. G Zhu, A Bax *J. Magn. Reson., Ser. A* **104** 353 (1993)
61. C H Gotfredsen, A Meissner, J Ø Duus, O W Sørensen *Magn. Reson. Chem.* **38** 692 (2000)
62. W Willker, D Leibfritz *Magn. Reson. Chem.* **33** 632 (1995)
63. K Furihata, H Seto *Tetrahedron Lett.* **40** 6271 (1999)
64. R T Williamson, B L Márquez, W H Gerwick, K E Kövér *Magn. Reson. Chem.* **38** 265 (2000)
65. K E Kövér, G Batta, K Fehér *J. Magn. Reson.* **181** 89 (2006)
66. A Bax, R Freeman *J. Am. Chem. Soc.* **104** 1099 (1982)
67. M Liu, R D Farrant, J M Gillam, J K Nicholson, J C Lindon *J. Magn. Reson., Ser. B* **109** 275 (1995)
68. G T Montelione, M E Winkler, P Rauenbuehler, G Wagner *J. Magn. Reson.* **82** 198 (1989)
69. G Wider, D Neri, G Otting, K Wüjthrich *J. Magn. Reson.* **85** 426 (1989)
70. A S Edison, W M Westler, J L Markley *J. Magn. Reson.* **92** 434 (1991)
71. A Bax, M F Summers *J. Am. Chem. Soc.* **108** 2093 (1986)
72. E M Tul'skaya, S N Senchenkova, L I Evtushenko, A S Shashkov, I B Naumova *Carbohydr. Res.* **340** 1247 (2005)
73. H Kogler, O W Sørensen, G Bodenhausen, R R Ernst *J. Magn. Reson.* **55** 157 (1983)
74. A A Grachev, A G Gerbst, N E Ustyuzhanina, A S Shashkov, A I Usov, N E Nifantiev *J. Carbohydr. Chem.* **25** 315 (2006)
75. A A Grachev, A G Gerbst, N E Ustyuzhanina, E A Khatuntseva, A S Shashkov, A I Usov, N E Nifantiev *J. Carbohydr. Chem.* **24** 85 (2005)
76. A A Grachev, A G Gerbst, N E Ustuzhanina, V B Krylov, A S Shashkov, A I Usov, N E Nifantiev *Mendeleev Commun.* **17** 57 (2007)
77. C Bauer, R Freeman, T Frenkiel, J Keeler, A J Shaka *J. Magn. Reson.* **58** 442 (1984)
78. H Kessler, U Anders, G Gemmecker, S Steuernagel *J. Magn. Reson.* **85** 1 (1989)
79. S Berger *Prog. Nucl. Magn. Reson. Spectrosc.* **30** 137 (1997)
80. R Freeman *Prog. Nucl. Magn. Reson. Spectrosc.* **32** 59 (1998)
81. D M Doddrell, D T Pegg, M R Bendall *J. Magn. Reson.* **48** 323 (1982)
82. D P Burum, R R Ernst *J. Magn. Reson.* **39** 163 (1980)
83. J Noggle, R E Schirmer *The Nuclear Overhauser Effect.* (New York: Academic Press, 1971)
84. A E Derome *Modern NMR Techniques for Chemistry Research* (Oxford: Pergamon Press, 1987)
85. A G Gerbst, N E Ustuzhanina, A A Grachev, E A Khatuntseva, D E Tsvetkov, A S Shashkov, A I Usov, N E Nifantiev *J. Carbohydr. Chem.* **21** 313 (2002)
86. J-R Brisson, J P Carver *Biochemistry* **22** 1362 (1984)
87. J Jeener, B H Meier, P Bachmann, R R Ernst *J. Chem. Phys.* **71** 4546 (1979)
88. R Wagner, S Berger *J. Magn. Reson., Ser. A* **123** 119 (1996)
89. S R Haseley, S G Wilkinson *Carbohydr. Res.* **306** 257 (1998)
90. R Eklund, G Widmalm *Carbohydr. Res.* **338** 393 (2003)
91. A A Bothner-By, R L Stephens, J Lee, C D Warren, R W Jeanloz *J. Am. Chem. Soc.* **106** 811 (1984)
92. A Bax, D G Davis *J. Magn. Reson.* **63** 207 (1985)
93. A Bax, D G Davis *J. Magn. Reson.* **65** 355 (1985)
94. S Mari, I Sánchez-Medina, P Mereghetti, L Belvisi, J Jiménez-Barbero, A Bernardi *Carbohydr. Res.* **342** 1859 (2007)
95. J P M Lommers, J J M van Rooijen, L M J Kroon-Batenburg, J P Kamerling, J F G Vliegenthart *Carbohydr. Res.* **337** 2279 (2002)

[a] — *Russ. J. Bioorg. Chem. (Engl. Transl.)*